NASA Contractor Report 182023

EXTENSION OF A THREE-DIMENSIONAL VISCOUS WING FLOW ANALYSIS

BERNARD C. WEINBERG
SHYI-YAUNG CHEN
STEPHEN J. THOREN
STEPHEN J. SHAMROTH

SCIENTIFIC RESEARCH ASSOCIATES, INC.
Glastonbury, Ct 06033

Contract NAS1-18140
MAY 1990

National Aeronautics and Space Administration

Langley Research Center
Hampton, Virginia 23665-5225

Table of Contents

SUMMARY

Three-dimensional unsteady viscous effects can significantly influence the performance of fixed and rotary wing aircraft. These effects are important in both flows about helicopter rotors in forward flight and flows about three-dimensional (swept and tapered) supercritical wings. A computational procedure for calculating such flow field is developed, and therefore would be of great value in the design process as well as in understanding the corresponding flow phenomena.

INTRODUCTION

In recent years there has been increased attention given to three-dimensional unsteady aerodynamics. Such flows manifest themselves over fixed wing and rotary wing aircraft. In regard to rotary wing aircraft, the helicopter operates in an unsteady environment. The flow about a helicopter rotor in forward flight is periodic as the blade passes through the rotor disc and the flow is characterized by its unsteady three-dimensional nature. Further, unsteady effects result from the wake vortex interaction due to the shed vortex of the preceding blade passing in the vicinity of the subject blade. In regard to fixed wing aircraft they are designed to be nominally steady, unsteady effects are introduced through either control surface motions or induced external oscillations. For both wing types these phenomena are observed throughout the Mach number regime; subsonic, transonic, and supersonic. The unsteady effects will influence loss levels as well as lift and moment coefficients which in turn influence the aeroelastic wing loading. For both type of wings the near wing flow may contain transonic shock wave boundary layer interactions as well as significant regions of reversed flow in the streamwise and spanwise directions. Obviously, a viscous analysis capable of treating unsteady, three-dimensional flows which may contain shock wave boundary layer interactions as well as regions of spanwise and streamwise reversed flow would be a significant aid to both the design and research engineer.

Concurrent with these needs there has been an increased effort to better understand these phenomena by conducting three-dimensional unsteady wing experimental programs (cf. Refs. 1, 2) and applying inviscid computational procedures to these programs (e.g. Refs. 3, 4). The results of the numerical calculations in conjunction with the experimental data indicate that the observed phenomena are strongly influenced by viscous effects near the body surface which are not accounted for by the inviscid predictions. These viscous effects are concentrated within a region that is predominantly thin except for localized regions of reverse flow in the streamwise and/or spanwise directions. Hence, there is clearly a need to compute these viscous effects in an efficient and economical manner.

There are several possible approaches available for computing three-dimensional viscous flows, ranging from empirical models to sophisticated treatments based on the solution of the three-dimensional time-dependent Navier-Stokes equations. Due to the complex structure of the flow the empirical

approach is too restrictive. At the other end of the spectrum is the three-dimensional time-dependent Navier-Stokes analysis. Even though such procedures have been developed at SRA and have been applied successfully to a variety of problems (e.g. Ref. 5), such a technique is not required for many of the viscous layer type problems occurring on wings in which the static pressure is sensibly constant across the viscous layer. Therefore, an approach is sought which allows the static pressure to be imposed at the boundary layer edge, but which can be used in three-dimensional flows having streamwise and/or crossflow separation.

A new computational procedure specifically designed to compute flow fields in which streamwise and/or spanwise separation is present, but in which the pressure is sensibly constant across the boundary layer has recently been developed (Ref. 6). This bridges the gap between the inviscid/boundary layer and Navier-Stokes approaches in that it is of sufficient generality to compute regions of reverse flow yet due to the imposition of pressure is considerably more economical than a full three-dimensional Navier-Stokes procedure. This technique was adopted to treat three-dimensional unsteady turbulent flows (Ref. 6). The results of this study are now described briefly.

Ref. 6 describes and demonstrates the implementation of a computer code for the efficient solution of three-dimensional time-dependent viscous flows on fixed and rotary wing aircraft. The numerical technique used is the Linearized Block Implicit (LBI) technique of Briley and McDonald (Refs. 7) in conjunction with QR operator technique (Refs. 8 and 9). This combination numerically solves the present approximate form of the turbulent Navier-Stokes equations which are derived for nonorthogonal coordinates in generalized tensor form. The rationale for the choice of this approach is discussed in detail in Refs. 6, 8 and 9.

The basic assumption made in the derivation of the governing equations is that the pressure does not vary normal to the shear layer, and is obtained from an inviscid analysis. Inherent in this assumption is that the shear layer is thin. Generally speaking, the boundary layer remains thin unless catastrophic flow separation occurs or the flow at the wing or rotor tip is considered. However, the analysis would apply to most of the wing or rotor under a range of operating conditions and thus represents an important tool.

It is also assumed at present that the stagnation temperature, T_o, is constant. This assumption is a good approximation for the flow fields considered as discussed in Ref. 5, and is included here only for purposes of computer run

economy. The full energy equation could equally well have been used in the analysis with consequent increase in computer run time. When the total temperature is assumed constant, the equation of state relates the density ρ to the velocity components u and w by an algebraic equation. The resulting formulation involves only the three velocity components, u, w and v and three equations, the streamwise and spanwise momentum equations and the continuity equation. Hence, a block-three system is considered. If T_o were calculated via the energy equation, a block-four system would result due to the inclusion of the temperature as an additional unknown and thus would result in an increase in computer run time.

For turbulent flows, a two-layer mixing length model is employed and its formulation in generalized tensor notation is given. A novel method is employed for solving the continuity equation in conjunction with the momentum equations. In Ref. 6, a complete description of the computational procedure is given, including coordinate systems, governing equations, turbulence model, and numerical technique, i.e. QR operator and Linearized Block Implicit schemes. The general outline of the computer code is also described.

The computational procedure has been validated by conducting computations with the numerical method referred to above and comparing it to the experimental data of Karlsson (Ref. 10), i.e. two-dimensional unsteady oscillating turbulent flow over a flat plate. Two-dimensional calculations were performed and the results agree both qualitatively and quantitatively with the data. Thereafter, the analogous three-dimensional case was considered which was obtained by a coordinate rotation to yield the flow over a plate skewed at 45° to the freestream direction. The results of this computation also agree well with both the two-dimensional results and Karlsson's data, hence validating the computational procedure in three dimensions. In addition, new inflow boundary conditions were developed and an explanation was proposed to resolve the controversy concerning other previously reported predictions of the skin friction phase lead angle as a function of reduced frequency. These results are described in detail in Ref. 6.

In this report, a description is given of the extension of the methodology to treat two-dimensional airfoils and three-dimensional wings. In order to achieve these applications a generalized three-dimensional nonorthogonal geometry formulation was developed. Also, the procedure was modified to calculate the flow through the wake. Examples of calculations conducted are presented.

DISCUSSION

To date, a computational procedure for three-dimensional unsteady viscous flows has been validated for three-dimensional unsteady oscillatory flow over a planar surface. The method was shown to be efficient and gave both qualitative and quantitative agreement with the experimental data. The major goal of the current effort was to extend this procedure so that it may be used routinely as an aid in the design of realistic fixed and rotary wing aircraft. This entailed in part the validation and extension of options in the computer code that were not exercised as yet and also required the incorporation of additional capabilities that would allow one to consider a more general class of flow phenomena consistent with current interests to both NASA and industry.

A major task required to complete the long term goal was to extend the geometrical capability of the computer code. The items considered were validation of the existing generalized nonorthogonal geometry option, extension of the geometrical capability to treat fully three-dimensional wings (with taper and sweep), and allow for transformations to account for boundary layer growth. Further, a method was developed to describe the wing surface, and to distribute the grid points throughout the domain to allow for the accurate solution of the governing equations. In the following section the governing equations and computational procedure are described. Thereafter a discussion is presented of the new methodology and the calculations that were conducted.

Computational Procedure

In describing the overall computational procedure, consideration is given to the governing equations: the turbulence model and the numerical algorithm. These topics are now briefly discussed.

Governing Equations

In the following, the governing equations are nondimensionalized as follows, x^i with respect to the characteristic length L, the velocity with respect to U_∞, density, pressure and temperature with respect to ρ_∞, $\rho_\infty U^2$ and $U_\infty{}^2/c_p$, respectively and time with respect to L/U_∞. The viscosity is nondimensionalized with respect to μ_∞.

Continuity Equation

$$\frac{\partial \rho}{\partial 1} + \frac{1}{J}\left[J\rho u^k\right]_{,k} = 0 \tag{1}$$

where J is the Jacobian, ρ the density, and u^k is the k^{th} contravariant velocity component.

Momentum Equations

The i^{th} momentum equation in the e_i direction is

$$\rho\left[\frac{\partial u^i}{\partial t} + u^k u^i \Big|_k\right] = -g^{ik}\left[\rho + \frac{2}{3}\frac{\mu}{Re}\Delta\right]_{,k} + g^{mk}\left[\frac{\mu}{Re}\, u^l\Big|_m\right]_k + g^{mi}\left[\frac{\mu}{Re}\, u^k\Big|_m\right]\Big|_k \tag{2}$$

where ',k' denotes a partial derivative, '|k' denotes a covariant derivative and g^{ik} is a component of the metric tensor.

In Ref. 12 it was pointed out that the QR Operator scheme requires that the governing equations be in quasi-linear form and that the spatial operator in a given direction operate on only one variable. For the momentum equation this requirement prevents the implicit treatment of certain diffusion terms that arise due to the curvature effects. In the usual boundary layer approximations these explicitly treated terms would not appear in the equation since they are of order $0\ (Re^{1/2})$ or smaller, and should, therefore be of little consequence.

Since mixed partial derivatives are commonly treated explicitly in orthogonal coordinate systems, this same approach is used in generalized nonorthogonal coordinates and this concept is extended to include mixed second covariant derivatives. All other second covariant derivatives are retained as implicit. Since the pressure is specified and impressed upon the viscous layer, its specification replaces the normal momentum equation. Thus, the streamwise and spanwise momentum equations are the only two retained. A more detailed discussion of the derivation of these equations is given in Ref. 12.

Energy Equation

For the energy equation, constant stagnation temperature is assumed. Neglecting the square of the normal velocity with respect to the squares of the other velocity components

$$T_o = T + \frac{1}{2}\left[u_p^2 + w_p^2\right] + \frac{g_{12}}{h_1 h_2} u_p w_p \tag{3}$$

where u_p and w_p are the physical velocity components. These assumptions are employed here only for simplification purposes. If warranted, they can be removed and the full energy equation can be considered.

Equation of State

The equation of state assumes a perfect gas and is given by

$$p = \frac{\gamma - 1}{\gamma} \rho T \tag{4}$$

Linearizations

The following analyses assume a set of linear partial differential equations. However, the convective part of the momentum equation and the continuity equation are nonlinear, containing terms that involve the product of density and velocity components. In order to overcome this difficulty, the procedure described in Ref. 12 is employed to linearize the aforementioned terms by Taylor series expansion about the known time level solution.

It is important to note that in the governing equations the contravariant velocity components are used. However, as noted in Ref. 12, it is advantageous to solve for the physical velocity components. Therefore, when the governing equations are subsequently cast into a form amenable to the application of the LBI scheme, they are transformed so that the physical velocity components appear.

Turbulence Model

In turbulent flow cases, the three-dimensional ensemble-averaged turbulent flow equations are considered. The approach taken here assumes an isotropic turbulent viscosity, μ_T, relating the Reynolds' stress tensor to mean flow gradients. Using Favre averaging (Ref. 15) the governing equations then are identical to the laminar equations with velocity and density being taken as mean variables and viscosity being taken as the sum of the molecular viscosity, μ, and the turbulent viscosity, μ_T.

At this point additional closure assumptions for the Reynolds stresses are required, i.e., the evaluation of μ_T. There are a variety of approaches available, from the simpler mixing length models to the more complicated one and two-equation models. Since the method is being applied to wall bounded cases, the mixing length model which has worked well in the past for similar flow environments (Ref. 16) was chosen. The extension to more complex models could be undertaken at a later time if warranted. At that time, the LBI procedure that is used for the solution of the momentum equation could be applied to the k and ϵ equations.

Employing the Prandtl mixing length concept, the turbulent viscosity is given as

$$\mu_T = \rho \ell^2 \sqrt{\Phi} \tag{5}$$

where ℓ is the mixing length and Φ is the dissipation function, which in generalized tensor notation is given by

$$\Phi = \frac{1}{2} e^{ij} e_{ij} \tag{6}$$

As in the Cartesian formulation, Φ does not automatically reduce to the dominant term for standard boundary layers, i.e., $\partial u/\partial y$ in two dimensions and $[(\partial u/\partial y)^2 + (\partial w/\partial y)^2]^{1/2}$ in three dimensions. Hence, provisions are made in the computer code that on option retain only the dominant components of the strain which would conserve computer time.

The mixing length formulation is based on McDonald's model (Ref. 17), and is given by

$$\ell = \ell_\infty \tanh \left[\frac{\kappa y}{\ell_\infty}\right] D \tag{7}$$

where ℓ_∞ is the outer layer length scale, and

$$D = i - \exp(-y^+/A^+) \tag{8}$$

where y^+ takes on its usual meaning. The constants appearing in Eqs. 7 and 8, κ, λ and A^+ are .4, .09 and 26.0, respectively, and δ is the local boundary layer thickness defined as .995 U_e. Note that in the limit as $y \to 0$, Eq. 7 reduces to

$$\ell_i = kyD$$

while for y, large Eq. 7 reduces to

$$\ell_o = \ell_\infty$$

the standard two layer values.

Numerical Procedure

The numerical procedure used to solve the governing equations is a consistently split linearized block implicit (LBI) scheme originally developed by Briley and McDonald (Ref. 15). The procedure is discussed in detail in Ref. 7. The method can be briefly outlined as follows: the governing equations are replaced by an implicit time difference approximation, optionally a backward difference or Crank-Nicolson scheme. Terms involving nonlinearities at the implicit time level are linearized by Taylor expansion in time about the solution at the known time level, and spatial difference approximations are introduced. The result is a system of multi-dimensional coupled (but linear) difference equations for the dependent variables at the unknown or implicit time level. To solve these difference equations, the Douglas-Gunn (Ref. 11) procedure for generating alternating-direction implicit (ADI) schemes as perturbations of fundamental implicit difference schemes is introduced in its natural extension to systems of partial differential equations. This technique leads to systems of coupled linear difference equations having narrow block-banded matrix structures which can be solved efficiently by standard block-elimination methods.

The method centers around the use of a formal linearization technique adapted for the integration of initial-value problems. The linearization technique, which requires an implicit solution procedure, permits the solution of coupled nonlinear equations in one space dimension (to the requisite degree of accuracy) by a one-step noniterative scheme. Since no iteration is required to compute the solution for a single time step, and since only moderate effort is required for solution of the implicit difference equations, the method is computationally efficient; this efficiency is retained for multi-dimensional problems by using what might be termed block ADI techniques. The method is also economical in terms of computer storage, in its present form requiring only two time-levels of storage for each dependent variable. Furthermore, the block ADI technique reduces multi-dimensional problems to sequences of calculations which are one-dimensional in the sense that easily-solved narrow block-banded matrices associated with one-dimensional rows of grid points are produced. A more detailed discussion of the solution procedure is discussed by Weinberg and McDonald (Ref. 12) and is given in Appendix B. In Appendix A the QR operator scheme is described which is used to obtain the spatial approximations. Further details can be found in Ref. 8.

Tasks Considered

The tasks considered in this contract are now described.

Geometric Modifications

This task pertained to the extension of the geometric capability of the computer code. In the existing computer code the metric tensor had a special form due to the fact that one coordinate is normal to the surface of the body and independent of the surface coordinates. Thus, the components $g_{i3} = g_{3i}$, for $i \neq 3$ are identically zero. This assumption restricted the ability to efficiently resolve boundary layers which have a significant variation of boundary layer thickness over the region of interest. If one wished to efficiently redistribute grid points normal to the wing by incorporating coordinate transformations that account for boundary layer growth, i.e. a y/δ transformation, where δ, the boundary layer thickness, is in general a function of the surface coordinates, then the metric tensor would become full. Since the new normal coordinate will be

a function of the streamwise and spanwise directions, g_{13} and g_{23} will be nonzero. Furthermore, the variation of the normal coordinate along the surface of the body will lead to corresponding nonzero Christofel symbols.

To achieve this enhanced generality and efficiency of the computer code the geometry arrays were expanded to include the additional nonzero entries and to accommodate the three-dimensional variation of the geometric coefficients. With regard to the computer code, several terms in the governing equations which were excluded previously were added to account for the new geometry.

Several computations were performed to validate the extended geometric capability. At this stage, the two-dimensional case considered in the Phase I effort, i.e., Karlsson's experimental data were recomputed using a y/δ transformation. The y/δ calculation considered is again the flat plate turbulent boundary layer, but now the outer boundary is permitted to grow at a prescribed rate. This allows for greater resolution near the upstream boundary by packing more points within the viscous layer.

Wake Wing Calculations

In the previous version of the computer code only one surface was treated, and that surface was a plane. For real wings, the surfaces are curved and both upper and lower surfaces must be treated as well as the wake. Hence, efforts were undertaken to modify the code and allow for the consideration of realistic geometries.

The first step undertaken was to define the airfoil shape. This involved the specification of a wing cross-section surface, i.e. thickness versus chord or distance from the leading edge. Afterwards the arc length was computed and grid points were distributed along the surface as desired from accuracy considerations. Several different types of airfoils are allowed, including the NACA 00XX series and the ONERA type sections. The code is sufficiently general to permit others, as well, for which either a formula is prescribed or y vs. x data is given. This procedure is employed for the upper and lower surfaces.

Of comparable importance is the viscous flow in the wake. The wake is obtained as an extension of the wing surface. That is, the centerline of the wake begins at the trailing edge and extends downstream several chord lengths, which in the cases considered, is somewhat further than three chord lengths. The outer edge of the computational domain is also prescribed at a fixed distance above the

surface, following the shape of the airfoil and for the wake region staying parallel to the centerline.

Two special features of the procedure are of note. First, the trailing edge region must be handled carefully. Since the geometric coefficients required by the calculation contain derivatives of the metric tensor, the metric tensor must remain smooth everywhere in the computational domain. For the trailing edge region this means that sharp angles are not permitted. Hence, the trailing edge was smoothed and a cusped region (zero slope) was added. Furthermore, the local radius of curvature was chosen such that the normal lines eminating from the concave surface would not intersect within the computational domain. Second, with regard to the wake centerline, in reality it is a double line consisting of the extensions of upper and lower surfaces. Special attention was given as is described subsequently.

Figure 1 shows a typical wing/wake coordinate system. The streamwise velocity is considered positive in the downstream direction from the leading edge for both the upper and lower surfaces. The normal velocity is considered positive directed away from the wall. Hence, the normal velocity on the upper surface is positive pointing up, while on the lower surface it is positive pointing down.

The solution procedure is described now. As noted previously, an Alternate Direction Linearized Block Implicit method is employed in the solution of the equation. In the first sweep, in the streamwise direction, the streamwise momentum equation is solved. For three-dimensional flow the spanwise momentum equation is also solved concurrently. First, the equations along these streamwise coordinate lines are solved for the upper surface and thereafter for the lower surface. The streamwise lines in these two regions extend from the leading boundary to the outflow or downstream boundary at the termination of the wake. This leaves only the wake "double line", which must be solved. The line extends from the trailing edge to the outflow boundary. Only one of these lines is computed, and the values are set on the other line. This completes the first sweep.

In the second sweep the equations are solved on the normal lines to the surface (cf. Figure 2). First the top surface and then the lower surface regions are computed until the onset of the wake region. In the wake additional manipulation of the equations are now performed since the entire region as a whole must be solved from the bottom to the top. This manipulation involves ordering the equations appropriately and accounting for the double line on the centerline

of the wake. At the boundary layer edges, above and below the airfoil, the streamwise velocity is specified as the boundary condition. On the wing surface no slip is specified, i.e. zero velocity. For three-dimensional flows, the spanwise edge velocity conditions are also specified similarly to the streamwise conditions at the boundary layer edge.

Different forms of boundary conditions are specified for the continuity equation. Since the continuity equation is discretized as a two point trapezoidal integral form, no boundary conditions as such are specified at the boundary layer edge but rather, the governing equation is solved there. However, at the centerline an additional condition is required. Since the velocity is not known there, *a priori*, it obviously cannot be specified. Instead, a smoothness condition is enforced, i.e., the second derivative of the normal velocity is set to zero. Note that for the momentum equation the governing equation itself is solved at the centerline.

Once the two sweeps are completed the velocity components are transformed into their physical normal to the wall and streamwise components.

Two-Dimensional Steady Turbulent Flow for NACA 0012 Airfoil

The case performed is the turbulent flow over a NACA 0012, symmetric airfoil at a 4.86° angle of attack. The freestream chord Reynolds number was .48E+07 and the mean freestream Mach number 0.599. The freestream temperature was assumed to be 300°K. The computational domain was chosen with inflow boundary located at $x = .1$ ft (.1 chord) and the outflow boundary located at $x = 4.6$ ft, while the outer edge was set to a constant value of .25 ft in the direction normal to airfoil surface for all x (the airfoil leading edge corresponds to $x = 0$ and trailing edge corresponds to $x = 1$). The grid distribution in the normal direction is based upon a hyperbolic tangent function. In the streamwise direction, a distribution based on series of error functions was used (Ref. 14). There were 49 mesh points distributed in the normal direction and 118 mesh distributed in the streamwise direction around the airfoil (62 grid points in the body region and 56 grid point in the wake region). From the pressure coefficients, the freestream velocity was calculated using isentropic relationships.

At $x = .1$, the inflow boundary, the displacement thickness of the upper and lower surfaces are assumed to be the same as that obtained from the integral

method, which are .60207E-03 ft and .33634E-03 ft, respectively.

The displacement thicknesses Reynolds numbers, $Re\delta^*$, at the above locations are therefore, 2800 and 2000, respectively, which can then be used to calculate the corresponding C_f via the Clauser formula

$$\sqrt{2/C_f} = 5.6 \log Re\delta^* + 4.3$$

The Cole's law velocity profile, i.e.:

$$\left.\begin{aligned} &\frac{u}{u_\tau} = \frac{1}{\kappa} \ln\left[\frac{yu_\tau}{\nu}\right] + C + \frac{2\pi(x)}{\kappa} \sin^2\left[\frac{\pi}{2}\frac{y}{\delta}\right] && \text{Wall-Wake Law} \\ &y^+ = u^+ && \text{Viscous Sublayer} \end{aligned}\right\} \quad (9)$$

where

$$y^+ = \frac{yu_\tau}{\nu} \quad , \quad u^+ = \frac{u}{u_\tau} \quad , \quad u_\tau = \sqrt{\tau_w/\rho}$$

and $\pi(x)/\kappa$ is evaluated from the condition that $u = u_\infty$ at $y/\delta = 1$; furthermore, constants κ and C are set at .41 and 5.0, respectively.

As described in Ref. 15, the relationship among $Re\delta^*$, δ, C_f, $\Pi(x)$ is

$$\frac{\kappa(Re\delta^* - 65)}{\delta U_\tau/\nu} = 1 + \Pi(x) \quad (10)$$

Eliminating $\Pi(x)$ from Eq. (9) and Eq. (10) yields

$$\frac{\bar{u}_\infty}{u_\tau} = \frac{1}{\kappa} \ln \lambda + \frac{2}{\lambda}\left[Re\delta^* - 65\right] - \frac{2}{\kappa} \quad (11)$$

where

$$\lambda = \delta u_\tau/\nu$$

The δ value, therefore, can be obtained from Eq. (11) by a Newton Ralphson iteration procedure which, together with C_f determines the required velocity profile. Once the streamwise velocity profiles are obtained the normal velocity

can be determined by assuming constant density for the purpose of setting upstream normal components and then integrating the continuity equation.

In the streamwise direction, the boundary layer option was employed, that is the streamwise diffusion terms were ignored and a backward difference approximation was used for the streamwise convective terms. The boundary conditions stipulated on the body surface were no-slip and zero normal velocity. At the outer edge of the viscous layer the magnitude of the streamwise velocity component was also prescribed. The value of the normal velocity component is not set, but rather computed as part of the numerical solution, as is the practice in standard boundary layer procedures. At the inflow boundaries, velocity profiles are fixed. Furthermore, the intermediate boundary conditions employed on the first sweep are the physical ones. For steady problems, the imposition of physical intermediate boundary conditions did not impair the quality of the solutions obtained. These results are in keeping with the analysis of McDonald and Briley (Ref. 15) for second order spatial scheme. A comparison between results obtained from VISTA 3-D and an integral method provided by NASA LARC personnel is shown in Figs. 3 and 4. Fig. 3 shows the displacement thickness as a function of distance along the airfoil. As can be seen, the agreement of predicted value between VISTA 3-D and the integral method for pressure side of the airfoil (lower surface) is excellent. For the suction side of the airfoil (upper surface), these two results were not in as close agreement, especially when x is large.

Similar curves for momentum thickness are shown in Fig. 4. Again, for the lower surface, the agreement is excellent; however, for the upper surface there was some disagreement between the two solution procedures, with the integral method overpredicting the values relative to the VISTA3D code.

Two-Dimensional Unsteady Turbulent Flow for NACA 0012 Airfoil

For the unsteady calculation the sample problem provided by NASA LARC personnel was a NACA 0012 symmetric airfoil which performs a sinusoidal pitching oscillation at the frequency of 4.789 Hz with amplitude of 1°. The freestream chord Reynolds number was .48E+07 and the mean freestream Mach number was .599. The procedure for obtaining unsteady flows is similar to the steady solution procedure. In the steady state case, the inflow and outer edge boundary conditions are prescribed to be invariant in time. For the unsteady case,

however, the velocities at these boundaries are allowed to change in time. At any instance the outer edge velocity is determined via the given pressure coefficient obtained from an inviscid calculation. In specifying the upstream velocity profile the present procedure adopts the same approach as does the steady state case. That is, the upstream profile is still given by the Cole's wall-wake velocity profile, but now C_f and δ^* are allowed to be periodic functions of time; i.e.,

$$C_f = C_{fo}(1 + AC_{f_1} \cos(\omega t + \phi_{C_f})) \tag{12}$$

where C_{f_o} and δ_o^* are the mean (time averaged) skin function and displacement thickness, C_{f_1} and δ_1^* are their respective amplitudes of oscillation and ϕ_{cf} and $\phi_{\delta *}$ their respective phase shifts. This procedure introduces additional unknowns. For the mean quantities C_{f_o} and δ_o^*, the steady state values are used. While the other four quantities are determined by the characteristics of the current problem. For this problem the oscillatory frequency, ω, is 4.789 Hz, the chord is 1 ft and the freestream velocity is 694 ft/s. Hence, the corresponding reduced frequency, based on chord, is .0433. This low reduced frequency implies that the quasi-steady flow is a valid assumption; physically this means that oscillatory changes are much slower than convection changes. For this reason, the phase angle ϕ_{cf} and $\Pi\tau\phi_{\delta *}$ in Eq. (9) would be insignificantly small and therefore is set to zero in the current study. Due to the quasi-steady characteristic, given the edge velocity in Cole's velocity profile the instantaneous C_f and δ would then be determined via the Newton-Ralphson iteration. In this study, however, a reasonable oscillatory amplitude would be given to C_f and δ^* to investigate the unsteady phenomena.

However, the low reduced frequency nature of the unsteady problem presents some constraints for the computations. First, the temporal discretizations are determined by the smallest time scale of the problem, i.e., the convective characteristics of the flow field. In general this means that for each time step that a particle in the freestream should not travel more than 10%-20% of the chord length. Based upon this criterion, approximately 1500 time steps are required in order to achieve temporal accuracy, significantly more time steps than were needed in the calculation of Ref. 6. As noted previously, 118 points were used in the streamwise direction. In order not to use an extensive amount of points in the trailing edge region, the inviscid pressure distribution was slightly modified to

diminish the large gradient there. This permitted the use of a coarser grid. Physically, one expects the inviscid pressure distribution to be higher than the viscous distribution, so that the aforementioned modification is not unreasonable. Thereafter, several test runs were performed to determine the optimum time increment that would not compromise the computational efficiency and numerical stability. The final selection of Δt is .00029 sec, which corresponds to nondimensional time steps of .208 (i.e. for each time increment a freestream particle would travel about 20% of the chord length) and 720 time steps per cycle.

It is noteworthy that in the Karlsson calculations (Ref. 6), due to the low freestream Mach number, the reduced frequency based on chord length was in the order of 1 to 10. For this reason, the time step could be determined from the external oscillatory frequency and therefore, 36 steps per cycle in most cases would produce satisfactory results. For a typical helicopter blade, the reduced frequency under normal operating condition is usually very low, hence the above-mentioned computational concerns would also be encountered. For comparison purposes a turbine blade, has a reduced frequency in the order of 1, and thus the aforementioned problems would not appear at all.

In presenting the results, the skin friction, C_f, the displacement thickness, δ^* and the streamwise velocity profile at the measuring station were Fourier decomposed into their harmonic components.

$$f(\tau) = \frac{a_o}{2} + \sum_{n=1}^{\infty} \left\{ a_n \cos\omega nt + b_n \omega nt \right\}$$

where

$$a_o = \frac{\omega}{\pi} \int_{t_1}^{t_1+T} f(\xi) \cos\omega n\xi \, d\xi$$

$$a_n = \frac{\omega}{\pi} \int_{t_1}^{t_1+T} f(\xi) \cos\omega n\xi \, d\xi$$

$$b_n = \frac{\omega}{\pi} \int_{t_1}^{t_1+T} f(\xi) \sin\omega n\xi \, d\xi$$

and where t_1 is the time at the start of the integration, and the period $T = 2\pi/\omega$.

Although the code allows for the determination of any number of harmonics, only the first two were obtained. Therefore, the Fourier series representation mean velocity is $a_o/2$, the in-phase component of the first harmonic is a_1 and the out-of-phase component of the first harmonic is $-b_1$. For the evaluation of the Fourier coefficients Simpson's integration scheme was used and all data points for the second cycle were sampled.

Table 1 is the result of the skin friction coefficient. It is seen from this table that the symmetry conditions (in the periodic sense) of the upper and lower airfoil is maintained, which is a necessary condition for the validity of the results. It is also seen that the mean skin friction coefficient is about fifty to one hundred times larger than the first harmonic oscillatory amplitude and the first harmonic amplitude is an order of magnitude larger than the second harmonic amplitude, which implies that for this particular problem the zero oscillatory amplitude of the friction coefficient for the upstream velocity profile is a valid assumption. Another interesting point is that the phase angle changes along the airfoil stations, which indicates that care must be taken to determine the upstream profile for a more general problem.

Table 2 and Table 3 present the Fourier analysis of the displacement thickness and momentum thickness, respectively. The general observations are similar to those of the skin friction coefficient, i.e.: 1) the symmetry conditions are satisfied; 2) the mean value is much larger than the oscillatory amplitude and the second harmonic oscillation is negligible; and 3) the phase angle is a function of location along the airfoil.

Table 4 shows the Fourier analysis of the streamwise velocity component at various stations along the normal direction at $x = .8$ (chord). It can be seen from this table that the mean value is the most important Fourier coefficient and therefore there is a significant phase shift from the wall to the outer edge.

The Fourier analysis of the pressure coefficient obtained from an inviscid analysis is shown in Table 5. As can be seen in this table the mean value and first harmonic amplitude of the pressure coefficient at the corresponding stations on the upper and lower surfaces are practically the same and the oscillatory angles are nearly 180 degrees out of phase. Furthermore, the amplitude of the first harmonic oscillation is about fifteen to twenty times larger than the second harmonic oscillation, indicating the first harmonic dominancy of this particular problem due to the small pitch oscillation.

y/δ Calculation

In order to test the nonorthogonal capability in two-dimensional and three-dimensional flows, several demonstration calculations were conducted. For the two-dimensional case, a y/δ calculation was undertaken for the incompressible turbulent flat plate flow. In previous calculations a cartesian coordinate system was employed, consisting of streamline and wall-normal coordinates. Since the boundary layer grows rather rapidly from leading to trailing edge; near the upstream boundary there would be very few points contained within the boundary layer. In order to cluster more points into the boundary layer, the outer edge was set at twice the local boundary layer thickness and allowed to grow at a $x^{\frac{1}{2}}$ rate. Thus, the 'streamwise' coordinate lines were no longer parallel to the wall but were curved, while the normal to the wall coordinates remained unchanged. Hence, the intersection of these two coordinates led to a full nonorthogonal coordinate system in which all geometries terms would be tested. It should be noted that in order to apply the method to generalized coordinates not only must one obtain the appropriate geometric coefficients, but one must compute the applicable velocity components. Since the governing equations are solved along coordinate lines, the physical velocity components must be transformed correctly to account for the curvature of the lines. Further, the pressure gradient term which is imposed on the boundary layer, at the outer edge was also accounted for to assure that one of the principal assumptions that the pressure remain constant through the layer (normal to wall) be enforced.

The results of the calculations for the nonorthogonal cases were compared to the cartesian case, with regard to velocity profile, skin friction coefficient displacement thickness and momentum thickness. These comparisons indicated that the results were well-behaved and given indistinguishable values, verifying the procedure. These modifications were then employed to compute the flow over a NACA 0012 airfoil.

Three Dimensional Unsteady Flow over a Skewed Nonorthogonal Coordinate System

For the three-dimensional calculation, the other aspect of the nonorthogonal coordinate system was investigated. In this case the nonorthogonality was limited to the surface, in the streamwise and spanwise directions instead of the normal/streamwise direction considered previously. The case undertaken was the

three-dimensional flow over a flat plate in which the streamwise flow is skewed to the leading edge at 45°. Fig. 5 shows the orthogonal case, which was studied in Ref. 6. In figure 6 is shown the case considered in the present study in which the streamwise coordinate lines are skewed at a 45° angle to the spanwise lines, and the normal lines to the surface remain normal. In this coordinate system all lines remain straight. The resulting spanwise velocity components in the new nonorthogonal system should remain zero. This indeed was the case for the calculation. The calculation was run in the steady and unsteady modes and the results compared well with the cartesian calculation.

Three-Dimensional Wing Studies

The first step in treating the flow over actual three-dimensional wings is to specify the geometry. This entails, as with the two-dimensional airfoils, the description of the wing cross-sectional shape, the specification of inflow and outflow boundaries and the boundary layer edge. A similar procedure to that which was used for the two-dimensional case was considered here for three-dimensions for specifying the surface and distributing the grid points. Please refer to that section for details. The one important difference for the three-dimensional case is that now, in addition to the streamwise and normal coordinate distribution, a spanwise distribution is required. Such a distribution is obtained by considering the wing consisting of a sequence of spanwise 2-D sections. The number is chosen from a consideration of the variation of spanwise shape; i.e., taper and sweep and the requirement of smooth geometric coefficients. Hence, the three-dimensional flow field is built up from a series of two-dimensional sections. An example of such a coordinate system is given in figures 7 to 13, in which an ONERA wing is shown.

Figures 7 and 8 are 2-D sections of the wing.

Figures 9, 10 and 11 are 3-D perspectives with spanwise coordinates on the wing and streamwise normal coordinates at the tip and root sections.

Figures 12 and 13 show the spanwise coordinates on the wing's surface. Note that the wing terminates at a fixed streamwise location.

Note that at the coordinate system begins .1 chord downstream of the leading edge where the inflow boundary conditions are specified.

The solution procedure is similar to the two-dimensional calculation with the exception that the spanwise momentum equation must be solved. This leads to a

three sweep method (see Appendix) with an increase in matrix block size.

As can be realized, the inclusion of a third dimension increases the complexity of the geometric specification since first and second variations of the metric need to be considered in three dimensions. For the skewed boundary layer described previously, although the streamwise and spanwise coordinate system was nonorthogonal, there was no curvature. This reduced the number of nonzero geometric terms. However, in the current cases where there is curvature of the coordinate lines, additional terms now present themselves. The entire geometry array was thus carefully checked for accuracy and smoothness. In order to verify the solution procedure a test case was constructed in which the entire three-dimensional flow code would be exercised, but in which the flow remains essentially two-dimensional. In this case the wing consisted of 5 identical spanwise planes (2-D airfoil sections), as shown in figures 10-13. First, the two-dimensional counterpart was solved in the steady state. This solution was used as the inflow boundary condition. At the other spanwise boundary (plane 5) an outflow boundary condition was set so that the first derivative velocity components was equal to zero. This boundary condition transforms the flow field to one which does not vary in the spanwise direction, thereby retaining a two-dimensional character. Calculations were conducted for this test case.

Although the flow field appeared to be two-dimensional through most of the flow field, there were regions where anomalous velocities appeared. Efforts were undertaken to discover the source of this problem. Unfortunately these efforts were not totally successful. Areas in the code were identified which could contribute to the observed results. In particular the computation of the source terms which arise from the evaluation of terms at the lagged time step were identified as the prime source. However, further work could not be conducted under the present contract. The results obtained to date are very encouraging and indicate that calculations of the type considered are realistic and attainable.

CONCLUSIONS

In this report, a method for solving unsteady flows over two- and three-dimensional wings was described. The initial computer code was extended to treat three-dimensional geometries in a nonorthogonal coordinate system containing coordinate lines with curvature terms. The entire wing is solved as a whole,

including the upper and lower surfaces and wake. The method was tested in two dimensions for the unsteady flow over a NACA 0012 airfoil. In three dimensions, the coordinate system, geometry and governing equations were extended to treat realistic wings. Although complete three-dimensional solutions were not obtained, this effort has laid the groundwork for the computation of such flow fields of interest.

REFERENCES

1. Sanford, M.C., Ricketts, R.H., Cazier, F.W. and Cunningham, H.J.: Transonic Unsteady Airloads on an Energy Efficient Transport Wing with Oscillating Control Surfaces, Journal of Aircraft, Vol. 18, No. 7, July 1981.

2. Ricketts, R.H., Sanford, M., Seidel, D.A. and Watson, J.J.: Transonic Pressure Distributions on a Rectangular Supercritical Wing Oscillating in Pitch, NASA TM 84616, March 1983.

3. Edwards, J.W., Bennet, R.M., Whitlow, W. and Seidel, D.A.: Time Marching Transonic Flutter Solutions Including Angle of Attack Effects, Journal of Aircraft, Vol. 20, No. 11, November 1983.

4. Yates, E.C., Wynne, E.C. and Farmer, M.G.: Effect of Angle of Attack on Transonic Flutter of a Supercritical Wing, Journal of Aircraft, Vol. 20, No. 10, October 1983.

5. Shamroth, S.J.: Calculation of Steady and Oscillating Airfoil Flow Fields via the Navier-Stokes Equations, AIAA Paper No. 84-0525, 1984.

6. Weinberg, B.C. and Shamroth, S.J.: Three-Dimensional Unsteady Viscous Flow Analysis over Airfoil Sections, NASA CR-172368, 1984.

7. Briley, W.R. and McDonald, H.: On the Structure and Use of Linearized Block ADI and Related Schemes. Journal of Comp. Physics, Vol. 34, No. 1, 1980.

8. Weinberg, B.C. and McDonald, H.: Solution of Three-Dimensional Time-Dependent Viscous Flows, Part 1: Investigation of Candidate Algorithms, NASA CR-166565, Part 1, 1979.

9. Weinberg, B.C. and McDonald, H.: Solution of Three-Dimensional Time-Dependent Viscous Flows, Part 2: Development of the Computer Code, NASA CR-166565, Part 2, 1980.

10. Karlsson, S.K.F.: An Unsteady Turbulent Boundary Layer, Journal of Fluid Mechanics, Vol. 5, 1959, pp. 622-636.

11. Douglas, J. and Gunn, J.E.: A General Formulation of Alternating Direction Methods, Numerische Math., Vol. 6, 1964, p. 428.

12. Weinberg, B.C. and McDonald, H.: Solution of Time-Dependent Viscous Flows, Part 3: Application to Turbulent and Unsteady Flows, NASA CR-166565, Part 3, 1982.

13. Oh, Y.H.: An Analytical Transformation Technique for Generating Uniformly Spaced Computational Mesh., NASA CP-2166, 1980, pp. 385-398.

14. Coles, D.E. and Hirst, E.A. (Editors): Proceedings Computation of Turbulent Boundary Layers - 1968. AFOSR-IFP Stanford Conference, Vol. 1, Compiled Data, 1969.

15. McDonald, H. and Briley, W.R.: Three-Dimensional Supersonic Flow of a Viscous or Inviscid Gas, Journal of Comp. Physics, Vol. 19, No. 2, 1974.

16. Favre, A.: Equations des Gaz Turbulents Compressibles, J. Mecanique, Vol. 4, pp. 361-392, 1965.

17. McDonald, H. and Camarata, F.J.: An Extended Mixing Length Approach for Computing the Turbulent Boundary Layer Development, Proceedings Computation of Turbulent Boundary Layers - 1968 AFOSR-IFP Stanford Conference, Vol. 1, pp. 83-98, 1969.

18. Ciment, M., Leventhal, S.H. and Weinberg, B.C.: The Operator Component Implicit Method for Parabolic Equations, J. of Comp. Physics, Vol. 28, 1978.

19. Berger, A.E., Solomon, J.M., Ciment, M., Leventhal, S.H. and Weinberg, B.C.: Generalized OCI Schemes for Boundary Layer Problems, Math. Comp., Vol. 35, No. 151, 1980.

20. Leventhal, S.J.: The Operator Compact Implicit Method for Reservoir Simulation, Proceedings of Fifth SPE Symposium on Numerical Reservoir Simulation, 1979.

21. Blottner, F.G.: Computational Techniques for Boundary Layers in "Computational Methods for Inviscid and Viscous Two- and Three-Dimensional Flow Fields," Fluid Dynamics Institute, Hanover, New Hampshire, 1975.

22. Weinberg, B.C., Leventhal, S.H. and Ciment, M.: The Operator Compact Implicit Scheme for Viscous Flow Problems. AIAA Paper No. 77-638. Presented at the 3rd AIAA Comp. Fluid Dynamics Conference, Albuquerque, NM, 1977.

23. Weinberg, B.C.: Viscous Flow Calculations Employing a Fourth Order Generalized Operator Compact Implicit Scheme, Paper 79-1468, Presented at 4th AIAA Comp. Fluid Dynamics Conference, Williamsburg, VA, 1979.

APPENDIX A

SPATIAL DIFFERENCE APPROXIMATIONS

QR Operator Notation

In this section, implicit tridiagonal finite difference approximations to the first and second derivatives and to the spatial differential operator are considered. The QR operator procedure for generating a variety of spatial discretizations is also introduced. As special cases, standard second-order finite differences, first-order upwind differences, fourth-order operator compact implicit (OCI), fourth-order generalized OCI and exponential type methods are obtained. Since all these schemes are of the same form (cf. below), a single subroutine which defines the difference weights is all that is required to identify the method, while leaving the basic structure of the program unaltered. The rationale for the use of the QR approach in the present problem is discussed in detail in Ref. 8.

The QR formulation allows for ADI methods and permits the treatment of systems of coupled equations, i.e., LBI methods. Although variable mesh schemes can be employed within the QR framework, it is believed preferable to use analytic transformations to obtain a uniform computational mesh, hence attention is restricted to uniform mesh formulations.

The general concepts and notation will be introduced for two-point boundary value problems and then the methodology will be extended to more general linear and nonlinear parabolic partial differential equations in one dimension. The application of QR operator method to multidimensional problems is discussed in the section pertaining to the LBI scheme.

Consider the two-point boundary value problem

$$\tilde{L}(u) = \tilde{a}(x)u_{xx} + \tilde{b}(x)u_x + \tilde{c}(x)u = \tilde{f}(x) \qquad \text{(A-1)}$$

with boundary values u(0) and u(1) prescribed. Derivative boundary conditions, although not discussed here, can easily be incorporated into the framework of the QR operator notation. Let the domain be discretized so that $x_j = (j-1)h$, $j = 1, 2, \ldots, J+1$, and $U_j \sim u(x_j)$, $F_j \sim u_x(x_j)$, $S_j \sim u_{xx}(x_j)$ and $h = 1/J$ is the mesh width. The numbering convention was chosen here to be compatible with FORTRAN coding.

Without loss in generality for $a(x) \neq 0$, Eq. (A-1) can be divided by $a(x)$ so that we may treat instead the following equation

$$L(u) = u_{xx} + b(x)u_x + c(x)u = f(x) \tag{A-2}$$

where

$$b(x) = \tilde{b}(x)/\tilde{a}(x),\ c(x) = \tilde{c}(x)/\tilde{a}(x) \text{ and } f(x) = \tilde{f}(x)/\tilde{a}(x)$$

Substituting the finite difference approximations to the first and second derivatives

$$\frac{D_o}{2h}U_j = \frac{U_{j+1} - U_{j-1}}{2h} = F_j = u_x(x_j) + O(h^2) \tag{A-3}$$

$$\frac{D_+D_-}{h^2}U_j = \frac{U_{j-1} - 2U_j + U_{j+1}}{h^2} = S_j = u_{xx}(x_j) + O(h^2) \tag{A-4}$$

into Eq. (A-2) and rearranging, we obtain

$$L(u) = \left[\frac{1}{h^2} - \frac{b_j}{2h}\right]U_{j-1} + \left[c_j - \frac{2}{h^2}\right]U_j + \left[\frac{1}{h^2} + \frac{b_j}{2h}\right]U_{j+1} = f_j \tag{14}$$

or

$$\left[1 - \frac{Rc_j}{2}\right]U_{j-1} + \left[h^2c_j - 2\right]U_j + \left[1 + \frac{Rc_j}{2}\right]U_{j+1} = h^2f_j \tag{A-5}$$

where $Rc_j = hb_j$ is the cell Reynolds number.

Equation (A-5) can be generalized by introducing operator format, i.e.

$$r_j^- U_{j-1} + r_j^c U_j + r_j^+ U_{j+1} = h^2(q_j^- f_{j-1} + q_j^c f_j + q_j^+ f_{j+1}) \tag{A-6}$$

where the superscripts (-) minus, (c) center, and (+) plus indicate the difference weight that multiplies the variable evaluated at the (j-1), (j) and (J+1) grid points respectively, and where the r_j's and q_j's for grid point j are functions of h, b_{j-1}, b_j, b_{j+1}, c_{j-1}, c_j and c_{j+1}. Comparing Eqs. (A-5) and A-6) we can identify the r_j's and q_j's, viz.,

$$\begin{aligned} r_j^- &= 1 - Rc_j/2 & q_j^- &= 0 \\ r_j^c &= h^2 c_j - 2 & q_j^c &= 1 \\ r_j^+ &= 1 + Rc_j/2 & q_j^+ &= 0 \end{aligned} \tag{A-7}$$

We now define the tridiagonal difference operators Q and R

$$\begin{aligned} R\left[U_j\right] &= r_j^- U_{j-1} + r_j^c U_j + r_j^+ U_{j+1} \\ Q\left[f_j\right] &= q_j^- f_{j-1} + q_j^c f_j + q_j^+ f_{j+1} \end{aligned} \tag{A-8}$$

Noting that L(u) = f and substituting Eq. (A-8) into Eq. (A-6), we obtain

$$R\left[U_j\right] = h^2 Q\left[f_j\right] = h^2 Q\left[L(u)_j\right] \tag{A-9}$$

Alternatively by employing the inverse operator Q^{-1} an expression for $L(u)_j$ can be obtained

$$L(u)_j = \frac{1}{h^2} Q^{-1} R U_j \tag{A-10}$$

For standard central finite differences $Q = Q^{-1} = I$, the identity matrix, so the spatial operator can be given explicitly in terms of U_{j-1}, U_j and U_{j+1}. However, in general, for higher order methods whereas Q is tridiagonal Q^{-1} is a full matrix, and the spatial operator cannot be given explicitly in terms of the variables at adjacent grid points. Hence, Eq. (A-10) provides a method for expressing the spatial operator for a wider class of difference approximations. The formalism in Eq. (A-10) is also applicable for first and second derivatives appearing alone (cf. Ref. 18). In Refs. 8 and 19 a technique due to Berger, et al. is described for constructing fourth order tridiagonal methods which possess a monotonicity property as the cell Reynolds number is increased, $R_c \to \infty$. This type of scheme is an option in the computer code.

APPENDIX B

LINEARIZED BLOCK IMPLICIT SCHEME

Consider a system of nonlinear partial differential equations

$$A\bar{\Phi}_t = \mathcal{D}\bar{\Phi} + \bar{\Psi} \tag{B-1}$$

where $\bar{\Phi}$ is a vector of unknowns and Ψ is a source term vector which is a function of x^1, x^2, x^3 and t. Extension to source terms which are functions of $\bar{\Phi}$ are discussed in Ref. 15. $\mathcal{D}$ is a three-dimensional nonlinear differential operator and the matrix A appearing in the momentum equations is equal to ρI where ρ is the density and I the unity matrix.

Equation (B-1) may be centered about the $n+\beta$ time level, i.e. $t^{n+\beta} = (n+\beta)\Delta t = n\Delta t + \beta\Delta t = t^n + \beta\Delta t$, and written

$$A^{n+\beta}\left[\bar{\Phi}^{n+1} - \bar{\Phi}^n\right]/\Delta t = \mathcal{D}^{n+\beta}\bar{\Phi}^{n+\beta} + \bar{\Psi}^{n+\beta} \tag{B-2}$$

where $0 \leq \beta \leq 1$ is a parameter allowing one to center the time step, i.e., $\beta = 0$ corresponds to a forward difference, $\beta = 1/2$ to Crank-Nicolson and $\beta = 1$ to a backard difference.

After linearizing Eq. (B-2) by Taylor series expansion in time about the n^{th} time level by the procedure described in Ref. 15 to give a second-order linearization, we obtain

$$A^n\left[\bar{\Phi}^{n+1} - \bar{\Phi}^n\right]/\Delta t = \mathcal{L}^n\left[\bar{\Phi}^{n+\beta} - \bar{\Phi}^n\right] - \mathcal{D}^n\bar{\Phi}^n + \bar{\Psi}^{n+\beta} \tag{B-3}$$

where $\mathcal{L}$ is the linearized differential operator obtained from $\mathcal{D}$.

The difference between the nonlinear operator $\mathcal{D}$ and the linear operator $\mathcal{L}$ is defined as $M^n = \mathcal{D}^n - \mathcal{L}^n$. At the intermediate level $n + \beta$, $\phi^{n+\beta}$ is represented as

$$\bar{\Phi}^{n+\beta} = \beta\,\bar{\Phi}^{n+1} + (1-\beta)\,\bar{\Phi}^n \tag{B-4}$$

Using these relationships and dropping the vector superbar for convenience a two-level hybrid implicit-explicit scheme is obtained

$$A^n(\Phi^{n+1} - \Phi^n)/\Delta t = \beta\mathcal{L}^n(\Phi^{n+1} - \Phi^n) + \mathcal{L}^n\Phi^n + M^n\Phi^n + \Psi^{n+\beta} \tag{B-5}$$

The vector $\psi^{n+\beta}$ represents all of the terms in the system of equations which are treated explicitly. More about this will be said later, but for the moment note that $\psi^{n+\beta}$ may be approximated to the requisite order of accuracy by some multilevel linear explicit relationship, or approximated by ψ^n with a consequent order reduction in temporal accuracy.

The operator $\mathcal{L}$ is now expressed as a sum of convenient, easily invertible suboperators $\mathcal{L} = \mathcal{L}_1 + \mathcal{L}_2 + \ldots . \mathcal{L}_m$. In the usual ADI framework these suboperators are associated with a specific coordinate direction. Further, it is supposed that these suboperators can be expressed in the QR notation introduced earlier. Writing $\psi^{n+\beta}$ and $M^n\phi^n$ as a single source term $S^{n+\beta}$, Eq. (B-5) is written as

$$A^n\left[\Phi^{n+1} - \Phi^n\right]/\Delta t = \beta\left[\mathcal{L}_1^n + \mathcal{L}_2^n + \mathcal{L}_3^n\right]\left[\Phi^{n+1} - \Phi^n\right] + \left[\mathcal{L}_1^n + \mathcal{L}_2^n + \mathcal{L}_3^n\right]\Phi^n + S^{n+\beta} \tag{B-6}$$

To solve this system efficiently it is split into a sequence of easily invertible operations following a generalization of the procedure of Douglas and Gunn (Ref. 18) in its natural extension to systems of partial differential equations. The Douglas-Gunn splitting of Eq. (B-6) is written as the following three-step procedure

$$A^n\left[\Phi^*-\Phi^n\right]/\Delta t = \beta\mathcal{L}_1^n(\Phi^*-\Phi^n) + \left[\mathcal{L}_1^n+\mathcal{L}_2^n+\mathcal{L}_3^n\right]\Phi^n + S^{n+\beta}$$

$$A^n\left[\Phi^{**}-\Phi^n\right]/\Delta t = \beta\mathcal{L}_1^n\left[\Phi^*-\Phi^n\right] + \beta\mathcal{L}_2^n\left[\Phi^{**}-\Phi^n\right] + \left[\mathcal{L}_1^n+\mathcal{L}_2^n+\mathcal{L}_3^n\right]\Phi^n + S^{n+\beta}$$

$$A^n\left[\Phi^{***}-\Phi^n\right]/\Delta t = \beta\mathcal{L}_1^n\left[\Phi^*-\Phi^n\right] + \beta\mathcal{L}_2^n\left[\Phi^{**}-\Phi^n\right] + \beta\mathcal{L}_3^n\left[\Phi^{***}-\Phi^n\right] + \left[\mathcal{L}_1^n+\mathcal{L}_2^n+\mathcal{L}_3^n\right]\Phi^n + S^{n+\beta} \qquad \text{(B-7)}$$

which can be transformed to the alternative form

$$\left[A^n-\Delta t\beta\mathcal{L}_1^n\right]\left[\Phi^*-\Phi^n\right] = \Delta t\left[\mathcal{L}_1^n+\mathcal{L}_2^n+\mathcal{L}_3^n\right]\Phi^n + \Delta t S^{n+\beta} \qquad \text{(B-8)}$$

$$\left[A^n-\Delta t\beta\mathcal{L}_2^n\right]\left[\Phi^{**}-\Phi^n\right] = A^n\left[\Phi^*-\Phi^n\right]$$

$$\left[A^n-\Delta t\beta\mathcal{L}_3^n\right]\left[\Phi^{***}-\Phi^n\right] = A^n\left[\Phi^{**}-\Phi^n\right]$$

If the intermediate levels are eliminated, the scheme can be written in the so-called factored form

$$(A^n-\beta\Delta t\mathcal{L}_1^n)(A^n)^{-1}(A^n-\beta\Delta t\mathcal{L}_2^n)(A^n)^{-1}(A^n-\beta\Delta t\mathcal{L}_3^n)(\Phi^{n+1}-\Phi^n) = \Delta t(\mathcal{L}_1^n+\mathcal{L}_2^n+\mathcal{L}_3^n)\Phi^n + \Delta t S^{n+\beta} \qquad \text{(B-9)}$$

The ADI formulation given in Eq. (B-8) is directly applicable for $\mathcal{L}_i$ operators represented in $Q^{-1}R$ operator format. Consideration of intermediate boundary conditions and the removal of the inverse operator Q^{-1} is given in Ref. 12.

It is worth noting that the operator $\mathcal{D}$ or $\mathcal{L}$ can be split into any number of components which need not be associated with a particular coordinate direction. As pointed out by Douglas and Gunn (Ref. 11), the criterion for identifying sub-operators is that the associated matrices by "easily solved" (i.e., narrow-banded). Thus, mixed derivatives and

complicating terms which might inhibit the use of OCI can be treated implicitly within such a framework, although this would increase the number of intermediate steps and thereby complicate the solution procedure.

An inspection of Eq. (B-8) reveals that only the linearized operators $\mathcal{L}_1^n$, $\mathcal{L}_2^n$ and $\mathcal{L}_3^n$ appear. Indeed, the computer code employs this feature by evaluating these three operators before the first sweep, storing them and accessing them as needed in the subsequent three sweeps. In addition, the terms arising from the nonlinear terms are immediately absorbed into $S^{n+\beta}$ as they appear, allowing for an efficient evaluation of the terms in the differential equations.

The spatial operators appearing in the differential equations $\mathcal{L}_1^n$, $\mathcal{L}_2^n$ and $\mathcal{L}_3^n$ must be identified at least formally in order to isolate the coefficients that are to be used in the construction of the Q and R operators. These operators can be represented in standard form at each grid point, i.e.,

$$\mathcal{L}_i^n \Phi_i^n = a_{i1}^n \Phi_{i,11} + a_{i2}^n \Phi_{i,1} + a_{i3}^n \Phi_i + a_{i4}^n \Phi_2 + a_{i5}^n \Phi_3 \qquad \text{(B-10)}$$

In Eq.(B-10) the first subscript of Φ indicates the velocity component (associated with the corresponding direction) and " , " indicates a derivative. The subscripts of the a_{ij}^n refer to the direction (i) and the term in the equation (j) respectively. Note that the equation is in quasi-linear form, since the coefficients of the derivative operators need to be identified, for use with the QR operator technique employed here. Alternate schemes have been proposed by Leventhal (Ref. 20) for equations in conservation form but are not considered here. In the following section, a description will be given of how this entire operator is discretized by employing the QR operator format, and how the discretization is incorporated into the LBI framework in order to solve the system of equations (B-8).

The continuity equation is considered first. Since it is a first-order partial differential equation it does not have the standard form of Eq. (B-9). Furthermore, in the linearization process ρ has been eliminated in favor of the u^i velocity components so that the continuity equation has become an equation for the three velocity components, and not density.

An inspection of the system of equations under consideration reveals that substantial savings can be realized if the equations are partioned appropriately. Due to the use of a boundary layer coordinate system, the normal velocity appears only in conjunction with terms associated with the normal "3" direction in the two momentum equations. Hence, in the first two sweeps where directions "1" and "2" are implicit one is required to solve only for the two corresponding velocity components in the streamwise and spanwise momentum equation without the need of considering the continuity equation. However, on the third sweep where all 3 velocity components appear, one must solve all 3 equations. This strategy reduces the solution procedure to the inversion of two 2 × 2 block matrices and one 3 × 3 block matrix rather than three 3 x 3 block matrices which leads to a substantial reduction in computation time. If the full Navier-Stokes equations were considered (including a normal momentum equation) the aforementioned partioning could not be applied since the normal velocity would appear in all three sweeps.

The question that arises is how to appropriately split the continuity equation, since it need only be solved on the third sweep. Here again the Douglas-Gunn formulation leads to the appropriate choice. The continuity equations written in conservation form is,

$$\frac{\partial \rho}{\partial t} + \frac{1}{J} \frac{\partial}{\partial x^l} \left[J \rho u^l \right] = 0 \tag{B-11}$$

After linearizing and eliminating ρ, the increment form is obtained

$$\begin{aligned} A^n \Delta u^{n+1} + B^n \Delta W^{n+1} + \frac{\Delta t \beta}{J} \frac{\partial}{\partial x^3} \left[v^n A^n \Delta u^{n+1} + v^n B^n \Delta w^{n+1} + \rho^n \Delta v^{n+1} \right] \\ = - \frac{\Delta t}{J} \frac{\partial}{\partial x^l} \left[J \rho u^l \right]^n + \frac{\Delta t \beta}{J} \frac{\partial}{\partial x^l} \left[(\rho^n + u^n A^n) \Delta u^{n+1} + (u^n B^n) \Delta w^{n+1} \right] \\ + \frac{\Delta t \beta}{J} \frac{\partial}{\partial x^2} \left[(\rho^n + w^n B^n) \Delta w^{n+1} + (w^n A^n) \Delta u^{n+1} \right] \end{aligned} \tag{B-12}$$

where all the velocity components are the contravariant components $u = u^1$, $w = u^2$ and $v = v^3$. J is the Jacobian and

$$A^n = \frac{\rho^n}{T^n}\left[g_{11}u^n + g_{12}w^n \right]$$

$$B^n = \frac{\rho^n}{T^n}\left[g_{22}w^n + g_{12}u^n \right]$$

By employing the Douglas-Gunn procedure, Eq. (B-12) is represented as a third sweep equation, and a consistent approximation is obtained to the continuity equation, i.e., the x^1 derivative term is evaluated at the * level and the x^2 derivative term is evaluated at the ** level. The values of the intermediate derivative terms are obtained after the solution of the first two sweeps of the two momentum equations. Note that these terms do not contain the normal velocity. The equation can thus be written in symbolic form

$$A^n\Delta u^{n+1} + B^n\Delta w^{n+1} + \frac{\Delta t\beta}{J}\frac{\partial}{\partial x^3}\left[J\left\{ A^n v^n \Delta u^{n+1} + v^n B^n \Delta w^{n+1} + \rho^n \Delta v^{n+1} \right\}\right] \qquad \text{(B-13)}$$

$$= S^n - \beta\frac{\Delta t}{J}\frac{\partial}{\partial x^1}\left[J\{\ \}\right]^* - \beta\frac{\Delta t}{J}\frac{\partial}{\partial x^2}\left[J\{\ \}\right]^{**}$$

Since the only term involving v is in the x^3 derivative term, one can directly integrate the equation with respect to x^3, i.e.

$$\int_{x^3}\left[A^n\Delta u^{n+1} + B^n\Delta w^{n+1} \right] dx^3 + \Delta t\frac{\beta\Delta t}{J}\left[v^n A^n \Delta u^{n+1} + v^n B^n \Delta w^{n+1} + \rho^n \Delta v^{n+1} \right]$$

$$= \int_{x^3}\left\{ S^n - \frac{\beta\Delta t}{J}\left[\ \right]^* - \frac{\beta\Delta t}{J}\left[\ \right]^{**} \right\} dx^3$$

The next section describes how this is done very easily via the QR operator scheme. The concept of integrating directly the continuity equation is not new. Davis (Ref. 21) in his coupled procedure for the solution of two-dimensional steady boundary layer equations used a trapezoidal rule to integrate the continuity equation. Weinberg (Refs. 22 and 23) also used a fourth-order Simpson integration scheme to solve the compressible boundary layer equations. Such procedures are stable and offer a viable alternative to approximating the derivatives by finite differences. Note that conceptually the continuity equation in integrated form is treated on each sweep of the Douglas-Gunn splitting, although in actuality this can be viewed as having the same form as each sweep and the integration operator can be incorporated into the $\mathcal{L}$ and $\mathcal{D}$ difference operators, and as a result the stability and consistency of the original splitting is retained.

	X Location (ft)	A0	A1	B1	A2	B2
Upper surface	0.10	.38967E-02	.67699E-07	-.22287E-06	.45814E-08	.45872E-08
	0.19	.42797E-02	-.17854E-05	.10715E-03	.17208E-05	.14361E-05
	0.28	.37928E-02	.18962E-04	.58182E-04	.22280E-05	.28273E-05
	0.37	.33806E-02	.25652E-04	.34367E-04	.16299E-05	.21941E-05
	0.46	.30506E-02	.31949E-04	.12734E-04	.18953E-05	.28714E-05
	0.55	.27747E-02	.33389E-04	-.39809E-06	.17504E-05	.28084E-05
	0.64	.25333E-02	.33425E-04	-.11757E-04	.57673E-06	.10136E-05
	0.73	.23010E-02	.31304E-04	-.20715E-04	.88873E-06	.16173E-05
	0.82	.20370E-02	.26728E-04	-.27119E-04	.54921E-06	.11568E-05
	0.91	.16355E-02	.22326E-04	-.36889E-04	.54578E-06	.13082E-05
Lower Surface	0.10	.38967E-02	-.65485E-07	.22272E-06	.51117E-08	.20698E-08
	0.19	.42784E-02	.14041E-05	-.10725E-03	.17291E-05	.26166E-05
	0.28	.37919E-02	-.19271E-04	-.58279E-04	.23958E-05	.34449E-05
	0.37	.33800E-02	-.26004E-04	-.34382E-04	.18662E-05	.24906E-05
	0.46	.30502E-02	-.32274E+04	-.12727E-04	.21981E-05	.29963E-05
	0.55	.27745E-02	-.33953E-04	.47986E-06	.20226E-05	.27750E-05
	0.64	.25332E-02	-.33865E-04	.11873E-04	.83414E-06	.85366E-06
	0.73	.23010E-02	-.31758E-04	.20835E-04	.11379E-05	.13654E-05
	0.82	.20372E+02	-.27238E-04	.27251E-04	.75024E+06	.85661E-06
	0.91	.16360E-02	-.22822E-04	.37076E-04	.70514E-06	.91072E-06

Table 1. Fourier coefficients of the skin friction coefficient, $M_\infty = .599$, $\alpha = 0^o$, $Re_\infty = .48 \times 10^7$, $\omega = 4.789$ Hz, Amplitude = 1^o.

	X Location (ft)	A0	A1	B1	A2	B2
Upper Surface	0.10	.37558E-03	.10251E-05	-.34408E-05	.41487E-07	.37172E-07
	0.19	.60572E-03	.90040E-05	-.14388E-04	-.72212E-06	-.77157E-07
	0.28	.88322E-03	.16692E-04	-.28909E-04	-.10799E-05	-.24535E-06
	0.37	.11733E-02	.23646E-04	-.42388E-04	-.12803E-05	-.29465E-06
	0.46	.14753E-02	.31001E-04	-.57202E-04	-.16526E-05	-.62924E-06
	0.55	.17918E-02	.37962E-04	-.72360E-04	-.18996E-05	-.84942E-06
	0.64	.21279E-02	.44949E-04	-.89561E-04	-.17706E-05	-.53297E-06
	0.73	.24990E-02	.51640E-04	-.10957E-03	-.23653E-05	-.11151E-05
	0.82	.29499E-02	.58006E-04	-.13420E-03	-.27464E-05	-.13336E-05
	0.91	.36501E-02	.68505E-04	-.17760E-03	-.36737E-05	-.21136E-05
Lower Surface	0.10	.37562E-03	-.10288E-05	.34379E-05	.48457E-07	-.26746E-08
	0.19	.60583E-03	-.90139E-05	.14406E-04	-.66228E-06	-.24148E-06
	0.28	.88345E-03	-.16711E-04	.28933E-04	-.96239E-06	-.57742E-06
	0.37	.11737E-02	-.23660E-04	.42403E-04	-.11091E-05	-.78803E-06
	0.46	.14758E-02	-.31013E-04	.57216E-04	-.14187E-05	-.12807E-05
	0.55	.17924E-02	.37951E-04	.72349E-04	-.16251E-05	-.16754E-05
	0.64	.21287E-02	-.44881E-04	.89528E-04	-.14518E-05	-.15477E-05
	0.73	.25000E-02	-.51517E-04	.10952E-03	-.19970E-05	-.23488E-05
	0.82	.29512E-02	-.57755E-04	.13411E-03	-.23460E-05	-.28170E-05
	0.91	.36521E-02	-.68062E-04	.17741E-03	-.32136E-05	-.40410E-05

Table 2. Fourier coefficients of the displacement thickness, M_{∞} = .599, $\alpha = 0^{o}$, $Re_{\infty} = .48 \times 10^{7}$, ω = 4.789 Hz, Amplitude = 1^{o}.

	X Location (ft)	A0	A1	B1	A2	B2
Upper Surface	0.10	.19396E-03	-.15819E-05	.53122E-05	.67836E-07	.28307E-07
	0.19	.36255E-03	.45777E-05	-.40789E-05	-.35501E-06	.97161E-07
	0.28	.54074E-03	.96275E-05	-.12559E-04	-.53417E-06	.91897E-07
	0.37	.72766E-03	.14538E-04	-.21068E-04	-.66937E-06	.64907E-07
	0.46	.92427E-03	.19361E-04	-.29917E-04	-.81875E-06	.21795E-07
	0.55	.11317E-02	.24066E-04	-.39249E-04	-.93101E-06	-.29324E-07
	0.64	.13532E-02	.28596E-04	-.49537E-04	-.10316E-05	-.12977E-06
	0.73	.15977E-02	.32907E-04	-.61394E-04	-.12272E-05	-.22583E-06
	0.82	.18904E-02	.37306E-04	-.76396E-04	-.14735E-05	-.40425E-06
	0.91	.23236E-02	.43333E-04	-.10003E-03	-.18755E-05	-.71813E-06
Lower Surface	0.10	.19391E-03	.15932E-05	-.53138E-05	.54570E-07	.87310E-07
	0.19	.36256E-03	-.45687E-05	.40855E-05	-.32827E-06	.50857E-07
	0.28	.54082E-03	-.96154E-05	.12566E-04	-.46961E-06	-.53037E-07
	0.37	.72781E-03	-.14520E-04	.21071E-04	-.56848E-06	-.17724E-06
	0.46	.92449E-03	-.19332E-04	.29916E-04	-.67790E-06	-.32197E-06
	0.55	.11320E-02	-.24020E-04	.39238E-04	-.75995E-06	-.47815E-06
	0.64	.13536E-02	.28516E-04	.49512E-04	-.83094E-06	-.69132E-06
	0.73	.15983E-02	-.32778E-04	.61346E-04	-.99498E-06	-.91953E-06
	0.82	.18911E-02	-.37094E-04	.76321E-04	-.12185E-05	-.12506E-05
	0.91	.23246E-02	-.43001E-04	.99899E-04	-.15864E-05	-.17971E-05

Table 3. Fourier coefficients of the momentum thickness, $M_\infty = .599$, $\alpha = 0^o$, $Re_\infty = .48 \times 10^7$, $\omega = 4.789$ Hz, Amplitude = 1^o.

Y Location (ft)	A0	A1*10E-02	B1*10E-02	A2*10E-09	B2*10E-04
.79905E-05	.04948	.06511	-.02223	.11204	.19723
.19971E-04	.12440	.16135	-.05247	.27655	.49104
.37933E-04	.22848	.27689	-.07411	.45449	.85434
.64861E-04	.33992	.35805	-.05323	.53970	1.10370
.10523E-03	.43214	.40067	-.01016	.53985	1.20040
.16575E-03	.50287	.42780	.03013	.51757	1.23020
.25645E-03	.55880	.44991	.06339	.48891	1.22900
.39237E-03	.60619	.47085	.09180	.45228	1.20170
.59630E-03	.64962	.49201	.11867	.40013	1.14100
.90094E-03	.69217	.51366	.14719	.32432	1.03670
.13572E-02	.73587	.53623	.17903	.22760	.89435
.20395E-02	.78255	.56236	.21255	.14362	.76938
.30582E-02	.83504	.59775	.24339	.14978	.78787
.45759E-02	.89799	.64677	.27354	.32806	1.07040
.68298E-02	.97582	.68939	.34904	.64044	1.50270
.10161E-01	1.05930	.60300	.67043	1.07000	2.11460
.15052E-01	1.08810	.30899	1.24970	-.33646	-.10069
.22161E-01	1.08860	.29894	1.26970	-.50781	-.33409
.32340E-01	1.08860	.29850	1.26970	-.50740	-.33452
.46615E-01	1.08860	.29791	1.26960	-.50683	-.33511
.66057E-01	1.08860	.29714	1.26940	-.50608	-.33586
.91504E-01	1.08860	.29622	1.26930	-.50656	-.33494
.12313E+00	1.08860	.29663	1.26910	-.53360	-.29539

Table 4. Fourier coefficients of the streamwise velocity component at $x = 0.64$ ft, $M_\infty = .599$, $\alpha = 0^o$, $Re_\infty = .48 \times 10^7$, $\omega = 4.789$ Hz, Amplitude = 1^o.

	X Location (ft)	A0	A1	B1	A2	B2
Upper Surface	0.00667	.37359E+00	.53143E-01	-.15568E+00	.55542E-02	.10341E-01
	0.02	-.16407E+00	.66513E-01	-.19742E+00	.57324E-02	.11953E-01
	0.10	-.50579E+00	.34666E-01	-.12677E+00	.28572E-02	.66401E-02
	0.20	-.48913E+00	.15502E-01	-.86272E-01	.12610E-02	.36559E-02
	0.30	-.42419E+00	.50351E-02	-.62910E-01	.77438E-03	.23653E-02
	0.40	-.35098E+00	-.10750E-02	-.47713E-01	.55894E-03	.16619E-02
	0.50	-.27876E+00	-.46788E-02	-.37000E-01	.45516E-03	.12288E-02
	0.60	-.20939E+00	-.66793E-02	-.28956E-01	.39502E-03	.92628E-03
	0.70	-.14071E+00	-.75418E-02	-.22558E-01	.35348E-03	.69629E-03
	0.80	-.66016E-01	-.75031E-02	-.17173E-01	.31613E-03	.50170E-03
	0.90	.32960E-01	-.67228E-02	-.12298E-01	.27679E-03	.31814E-03
	1.00	.13490E+00	-.65013E-02	-.11328E-01	.26991E-03	.27956E-03
	2.35	.25901E-01	-.32397E-03	-.69127E-05	.33794E-04	-.58784E-04
	4.259	.64130E-02	-.39253E-03	-.14794E-03	.36091E-04	-.11784E-04
Lower Surface	0.00667	.37234E+00	-.52208E-01	.15568E+00	.63076E-02	-.90089E-03
	0.02	-.16566E+00	-.65501E-01	.19744E+00	.66513E-02	-.23155E-02
	0.10	-.50644E+00	-.34047E-01	.12677E+00	.31258E-02	-.25283E-02
	0.20	-.48916E+00	-.15117E-01	.86259E-01	.11151E-02	-.25727E-02
	0.30	-.42390E+00	-.47297E-02	.62885E-01	.41961E-03	-.21672E-02
	0.40	-.35051E+00	.13454E-02	.47677E-01	.96358E-04	-.17663E-02
	0.50	-.27820E+00	.49352E-02	.36959E-01	-.56707E-04	-.14269E-02
	0.60	-.20880E+00	.69319E-02	.28902E-01	-.12427E-03	-.11465E-02
	0.70	-.14015E+00	.77983E-02	.22496E-01	-.14360E-03	-.91693E-03
	0.80	-.65507E-01	.77729E-02	.17100E-01	-.13505E-03	-.72658E-03
	0.90	.33374E-01	.70029E-02	.12215E-01	-.99902E-04	-.56533E-03
	1.00	.13529E+00	.67711E+02	.11241E-01	-.89012E-04	-.53487E-03
	2.35	.25919E-01	.38366E-03	.10067E-03	.20206E-04	-.55207E-04
	4.259	.64370E-02	.46165E-03	.10643E-03	.18169E-04	-.22176E-04

Table 5. Fourier coefficients of the outer edge free stream pressure coefficient, $M_\infty = .599$, $\alpha = 0^o$, $Re_\infty = .48 \times 10^7$, $\omega = 4.789$ Hz, Amplitude = 1^o.

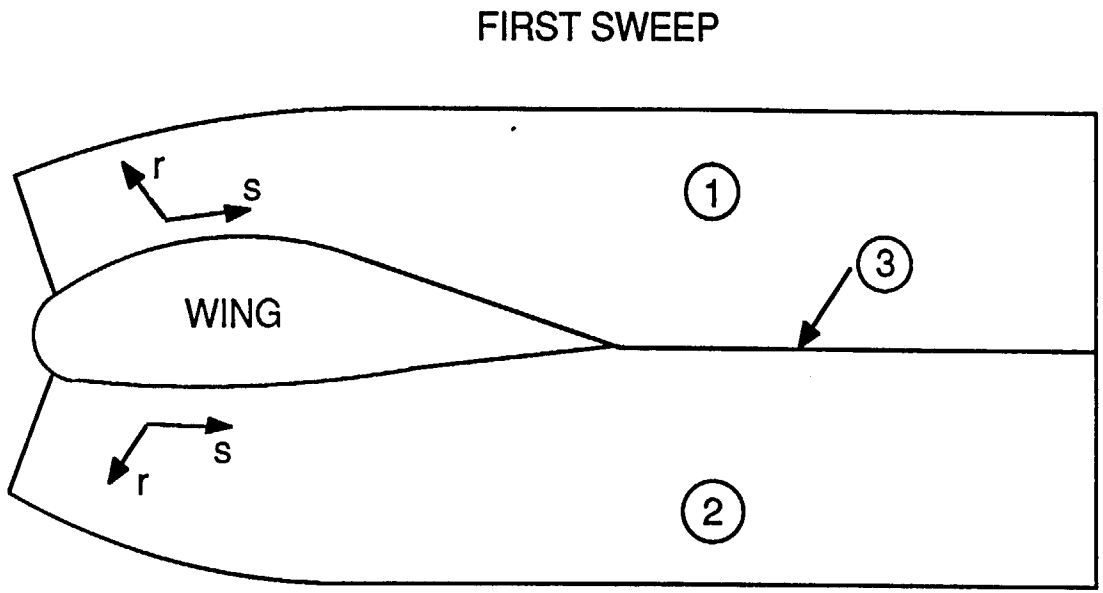

REGION (1) UPPER SURFACE

REGION (2) LOWER SURFACE

REGION (3) WAKE CENTERLINE

Figure 1. First Sweep Coordinates

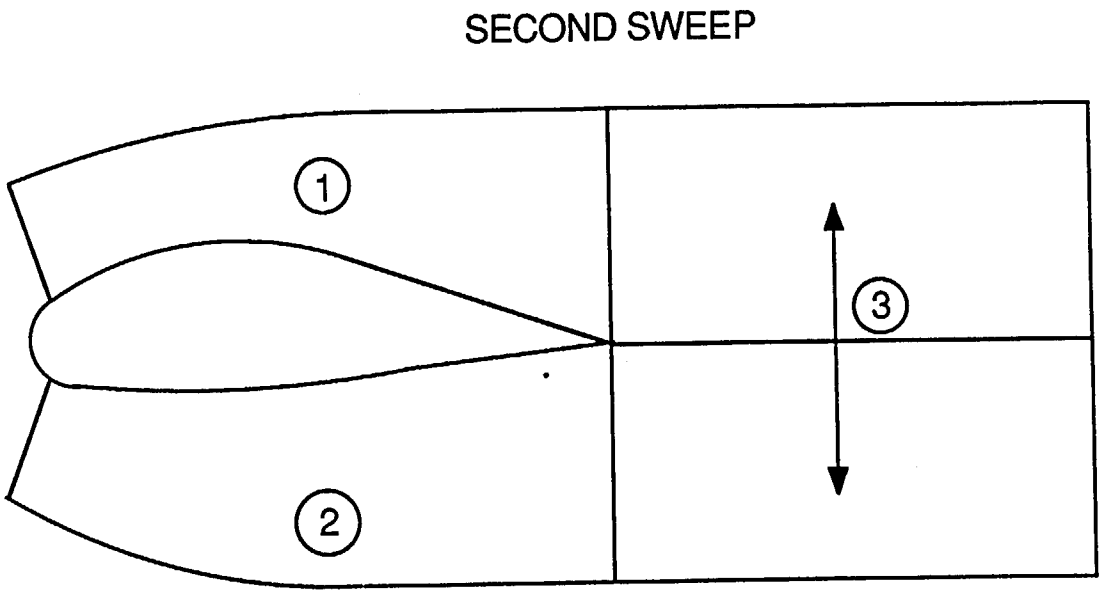

Figure 2. Second Sweep Coordinates

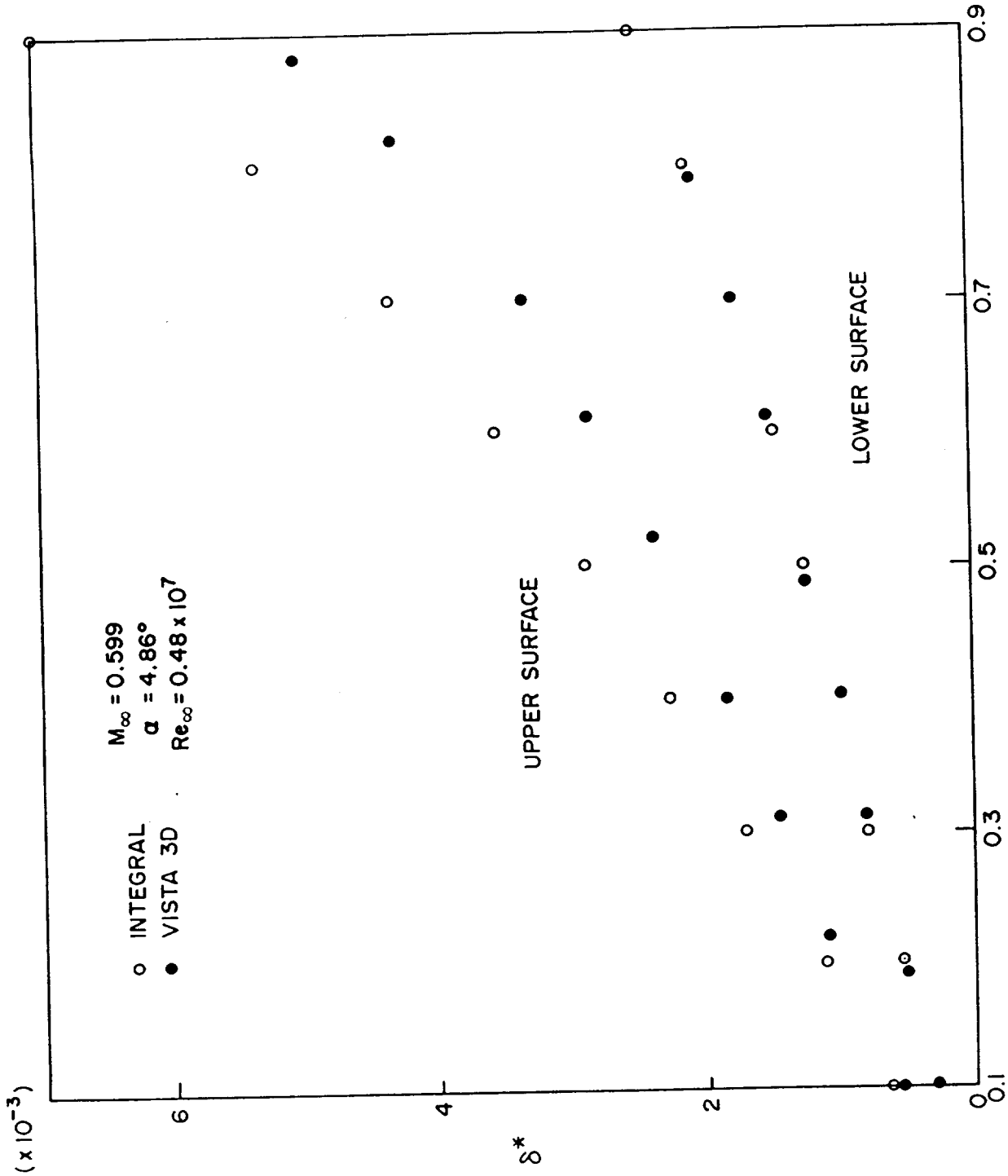

Figure 3. Displacement Thickness Distribution on NACA 0012 Airfoil

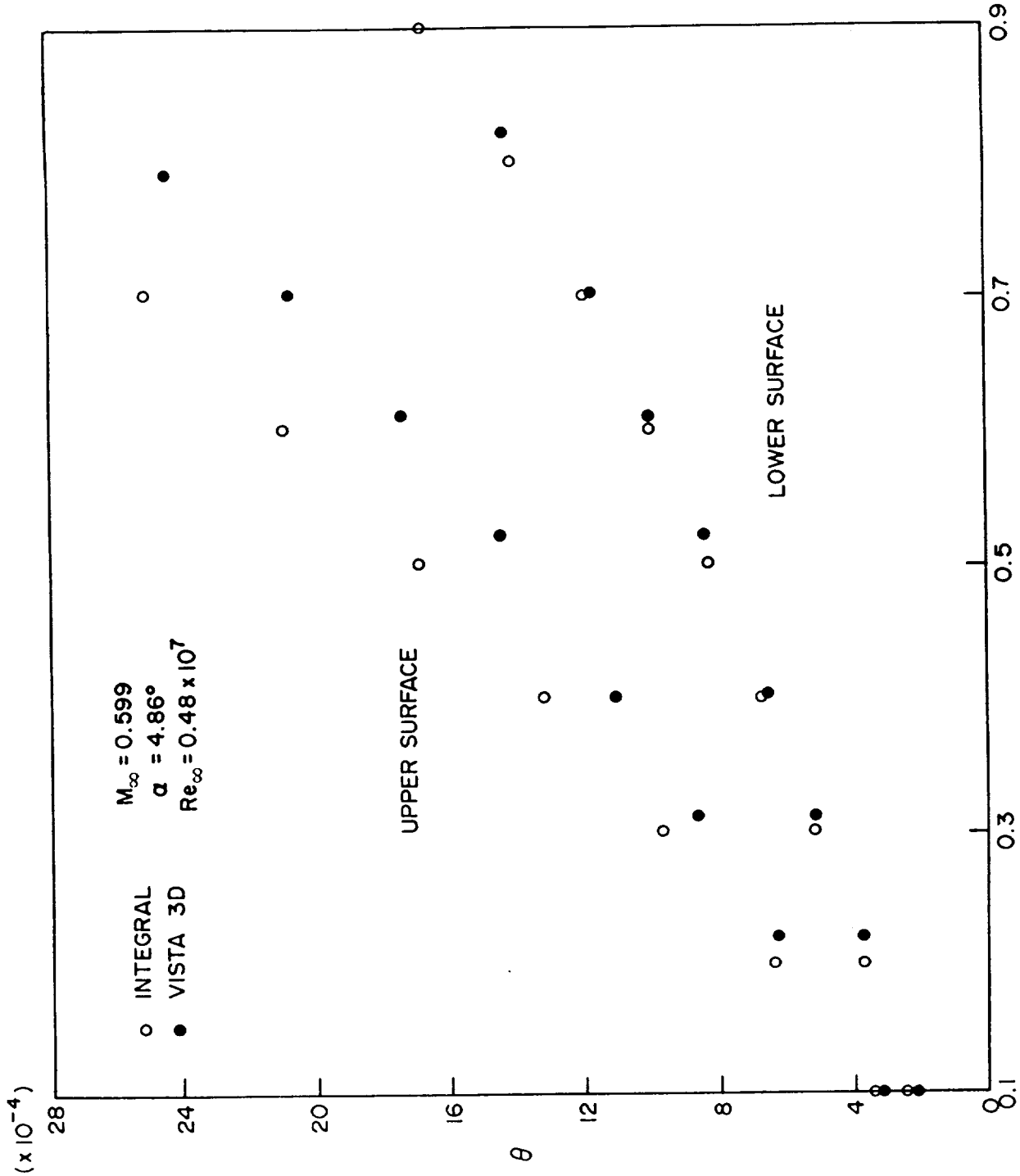

Figure 4. Momentum Thickness Distribution on NACA 0012 Airfoil.

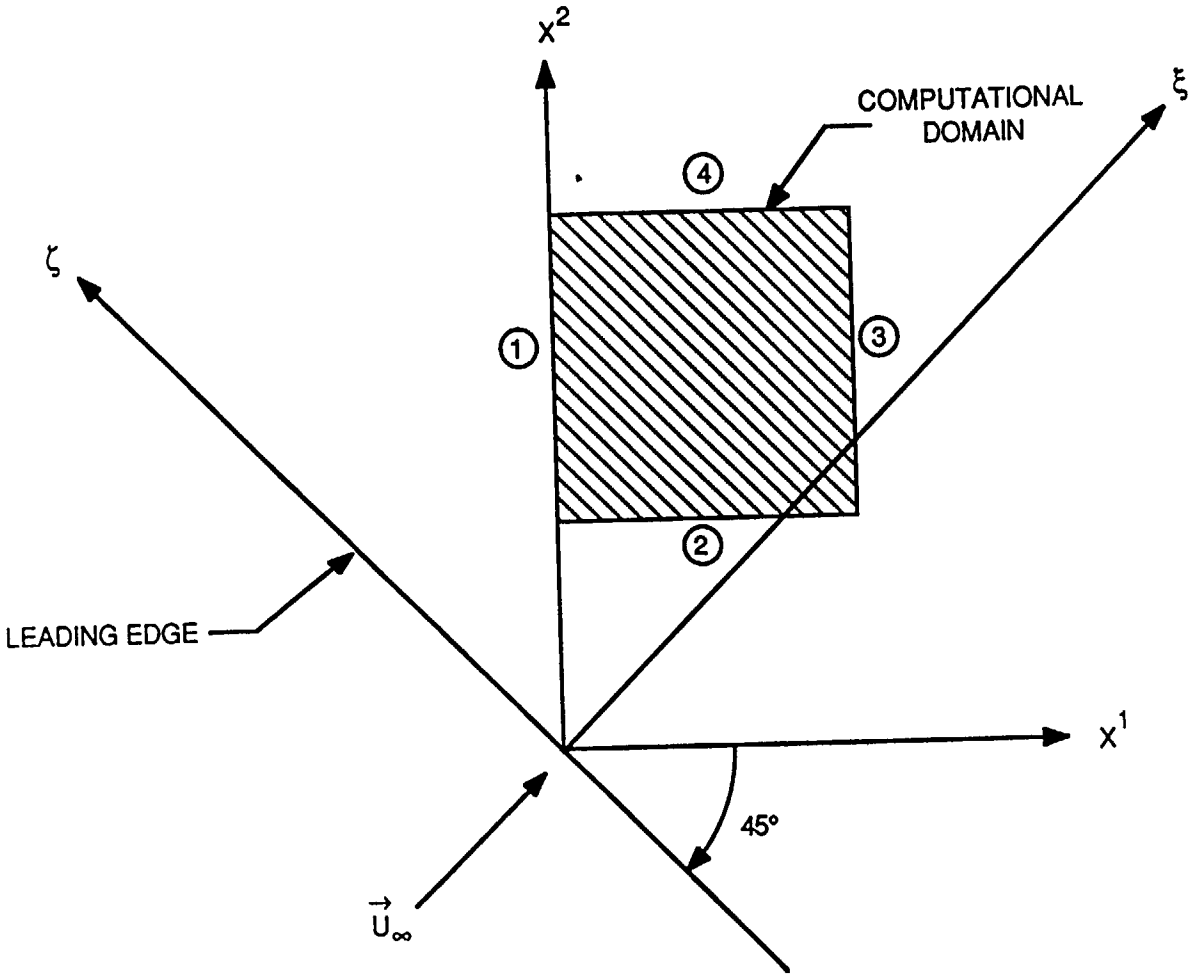

Figure 5. Three-Dimensional Computational Domain.

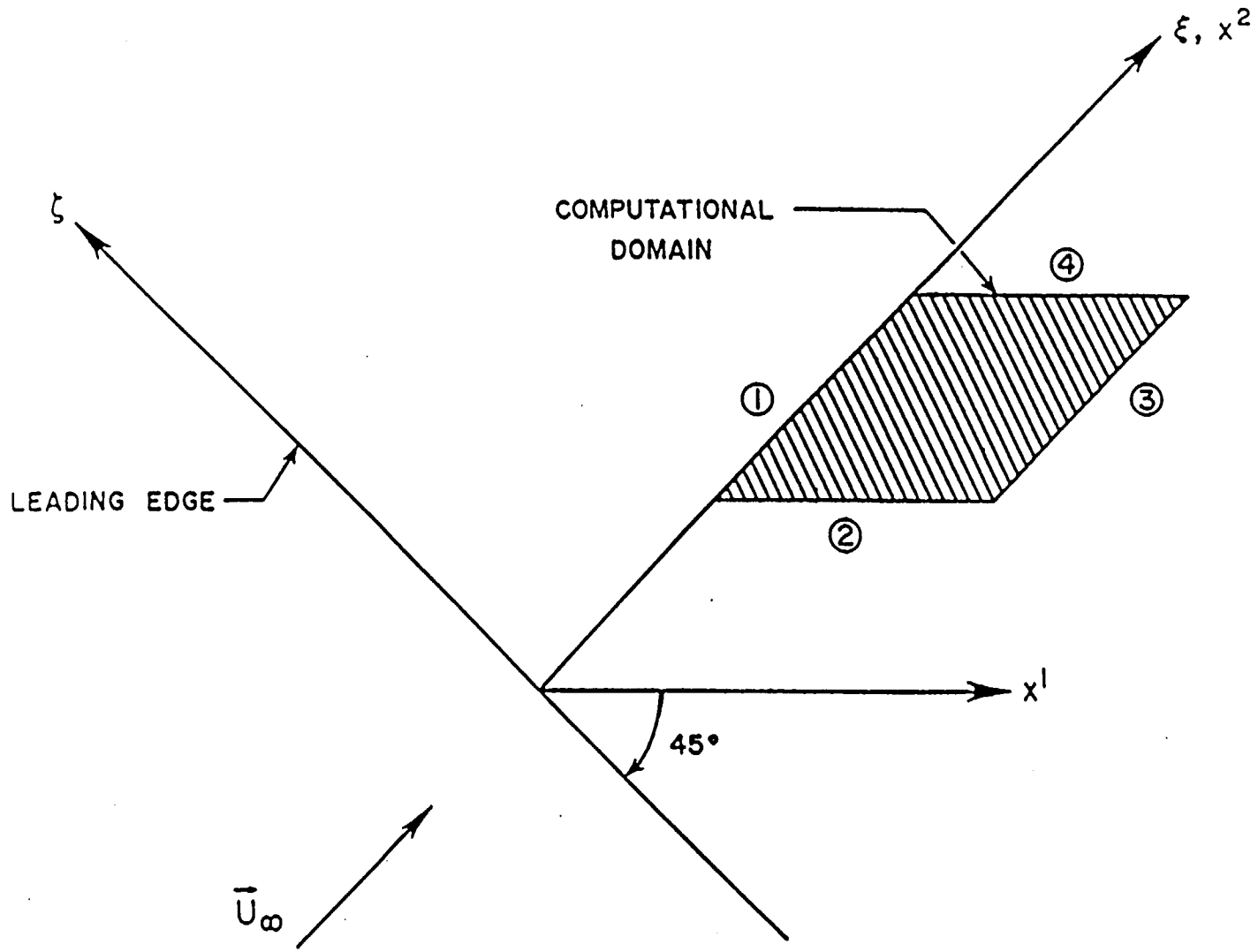

Figure 6. - Three-Dimensional Computational Domain for Nonorthogonal Coordinates

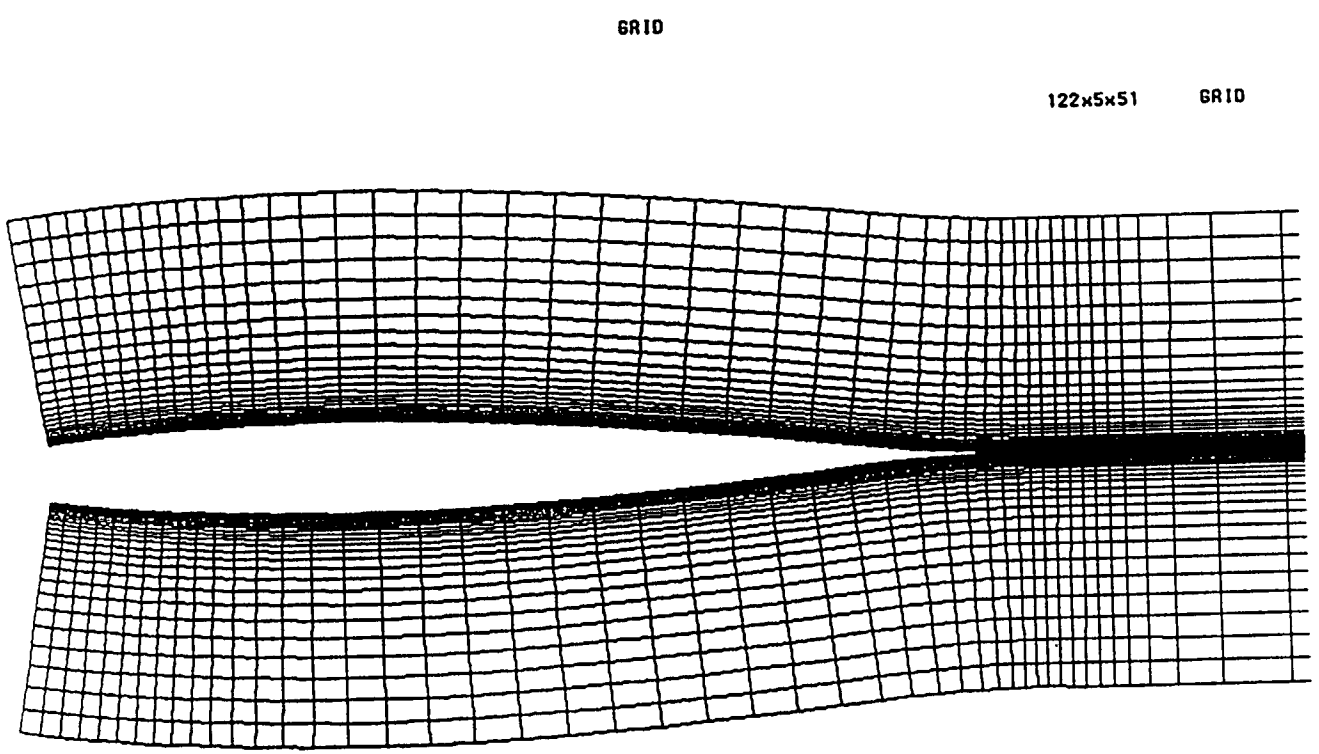

Figure 7. Two-Dimensional Section

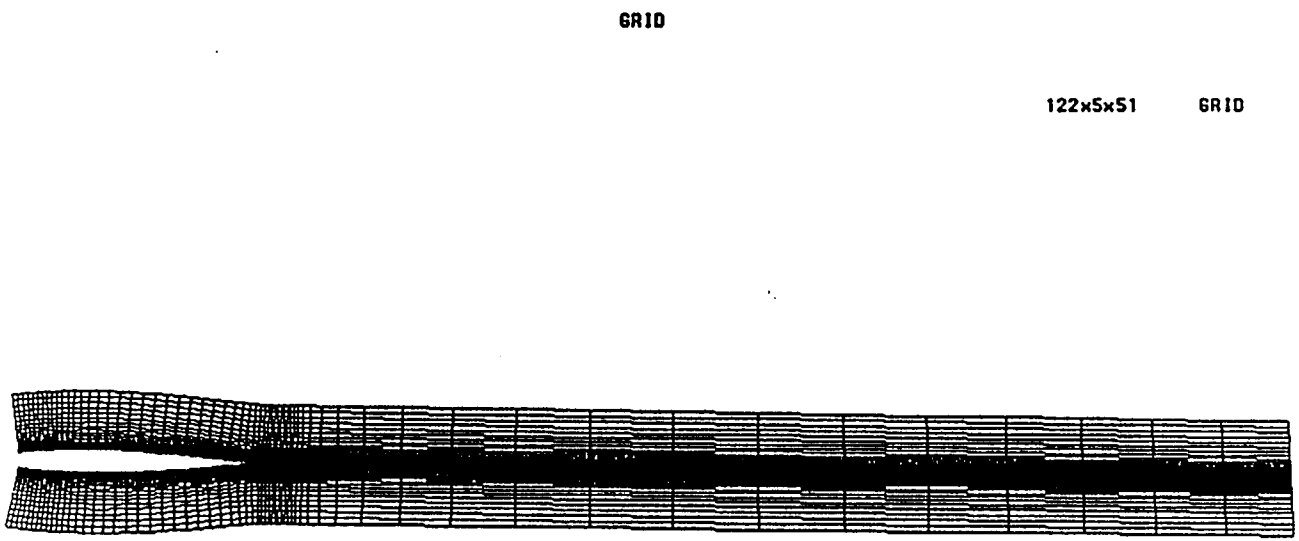

Figure 8. Two-Dimensional Section with Wake

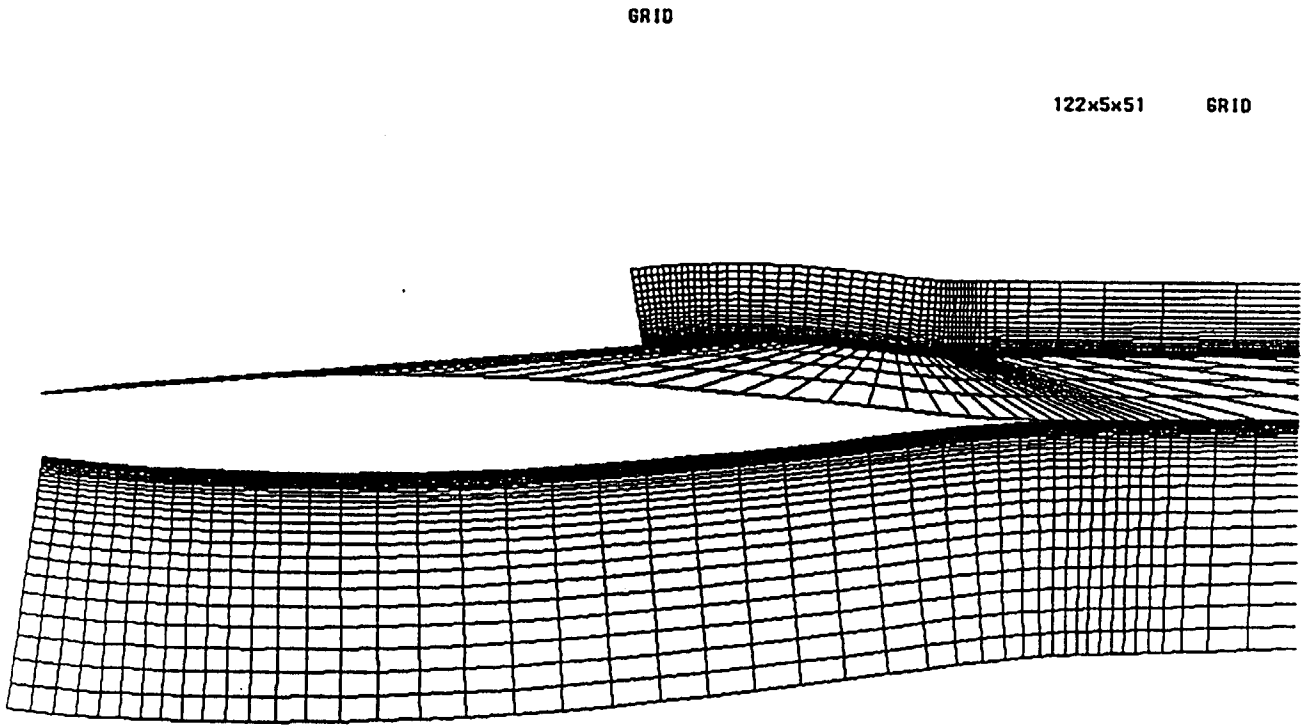

Figure 9. 3-D Perspective of Wing Side View

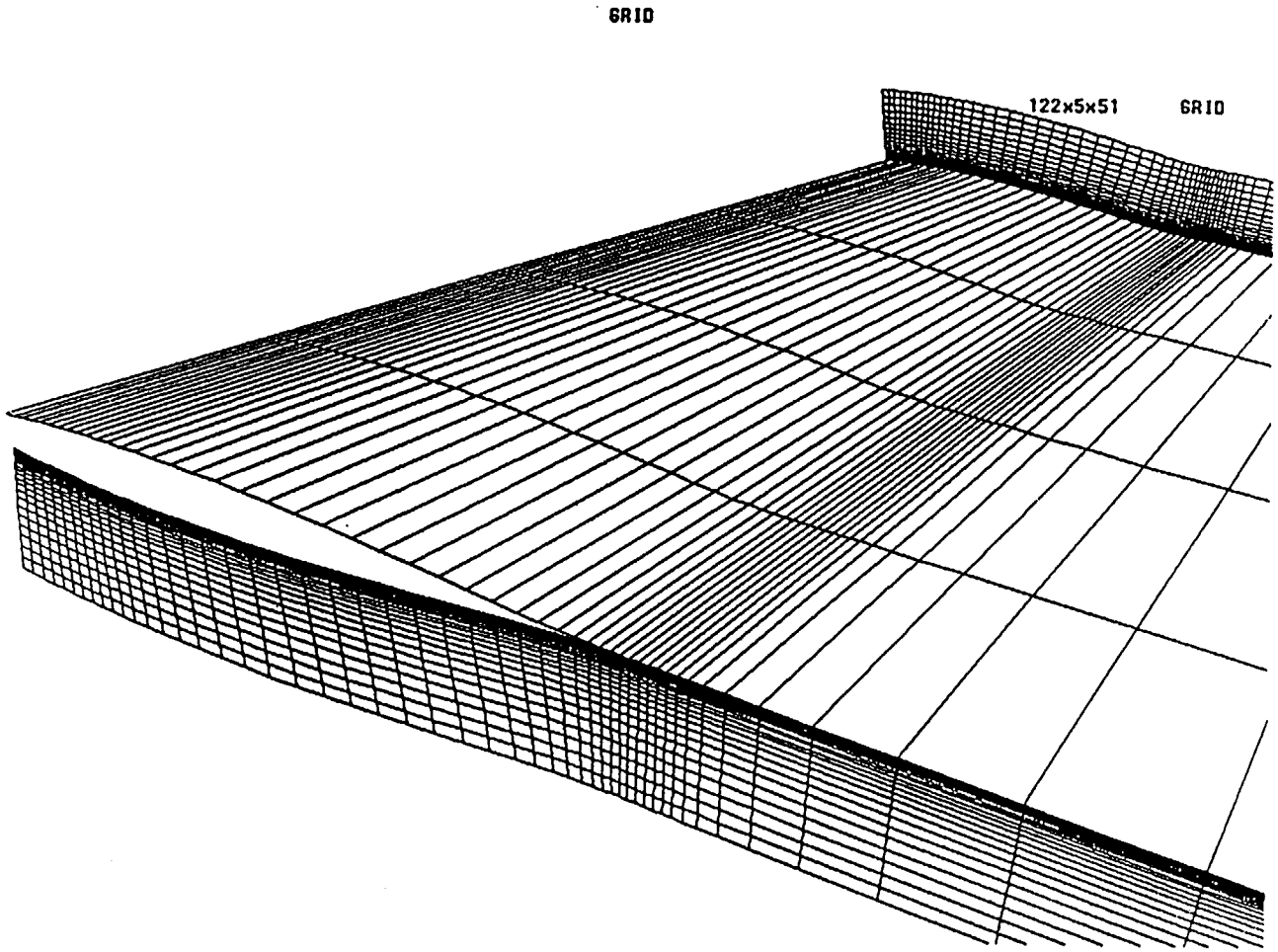

Figure 10. 3-D Perspective of Wing Top View

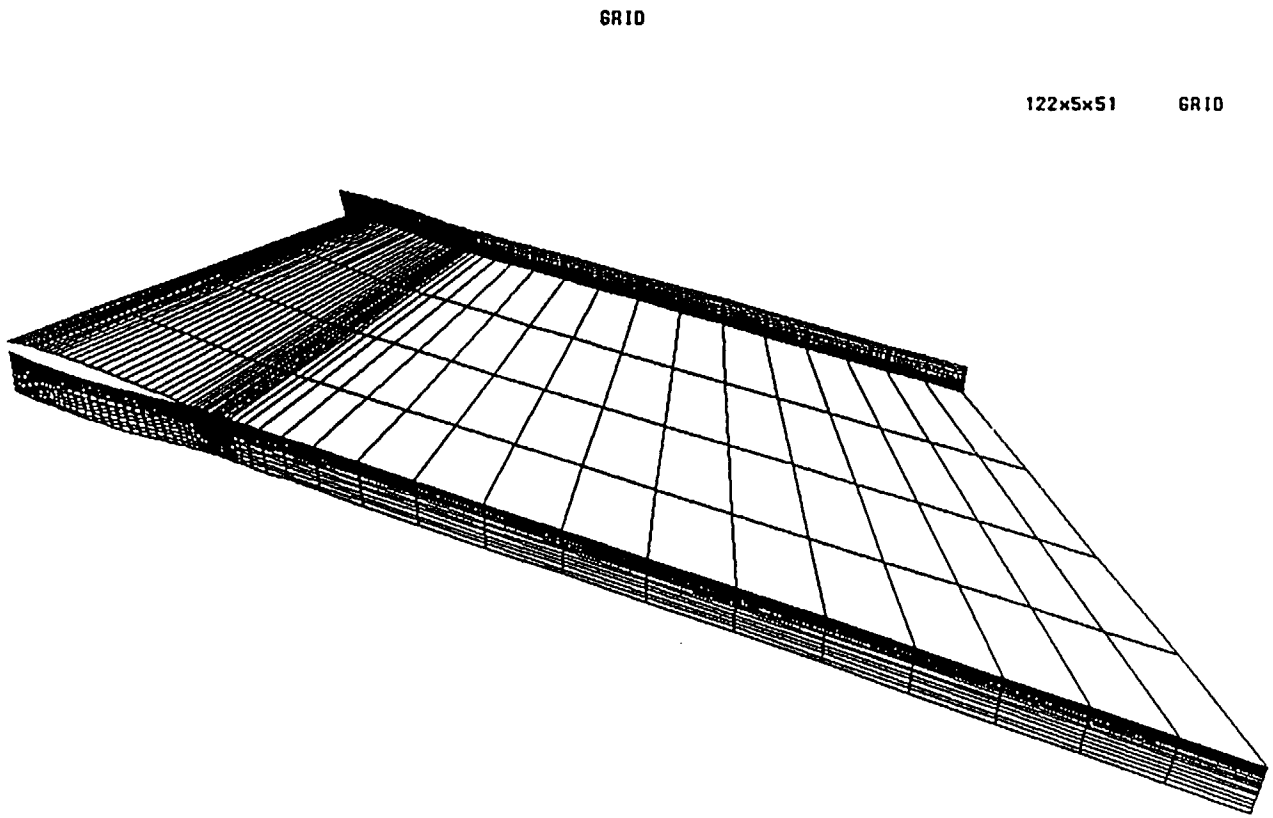

Figure 11. 3-D Perspective with Wake

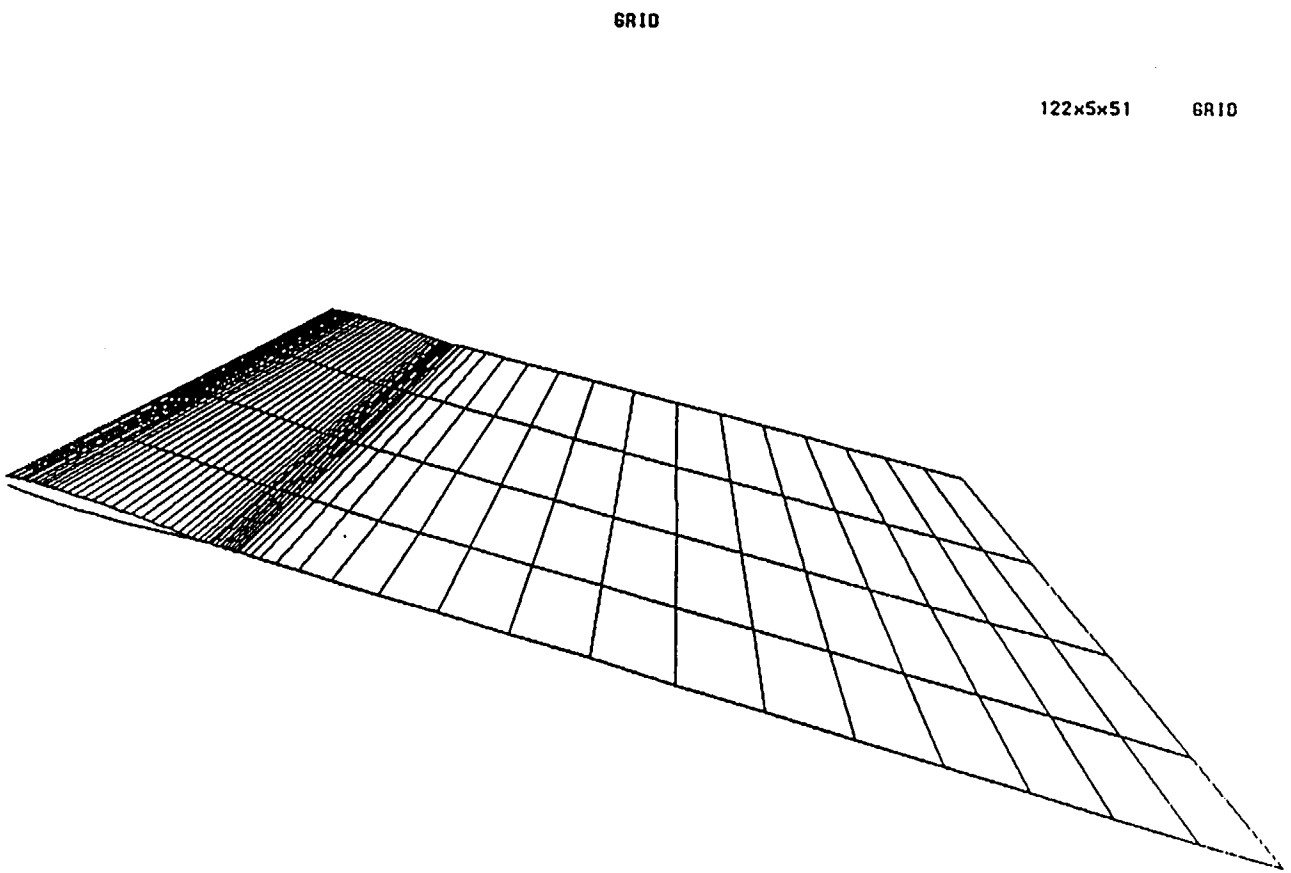

Figure 12. Spanwise Coordinates

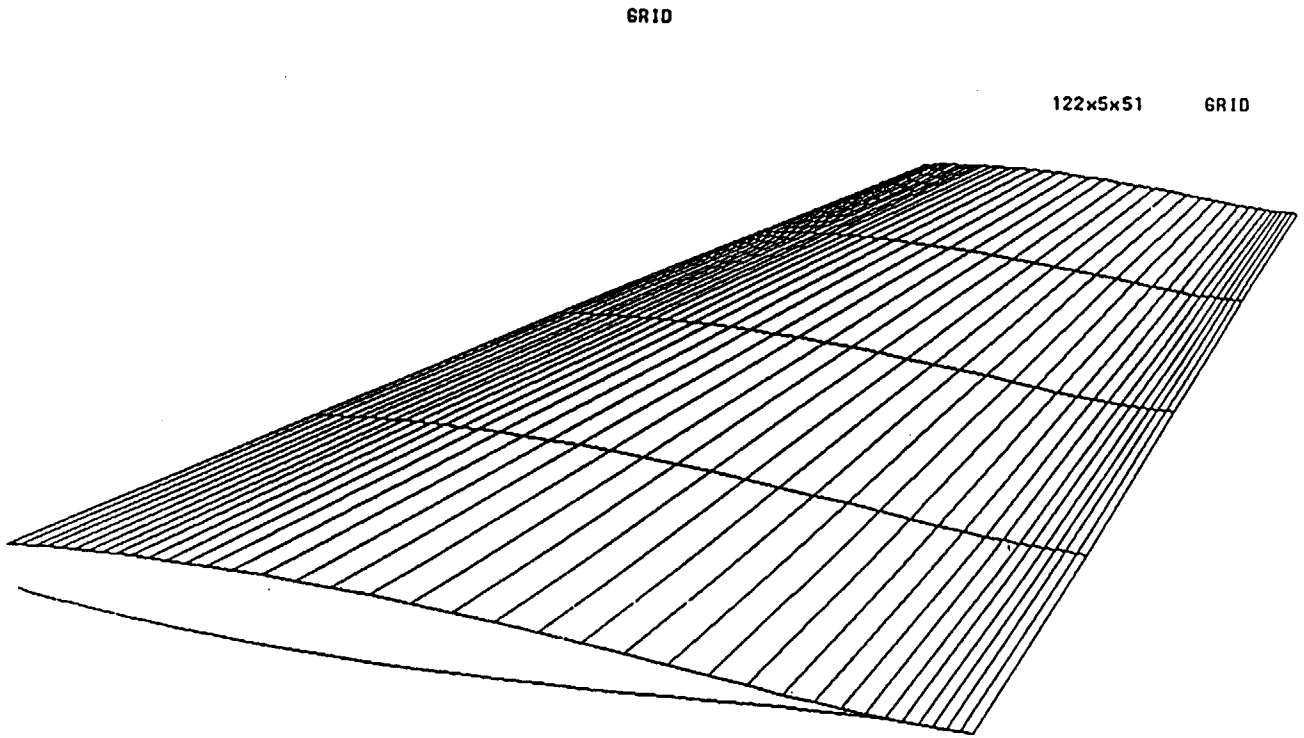

Figure 13. Spanwise Coordinates

NASA National Aeronautics and Space Administration

Report Documentation Page

1. Report No.	2. Government Accession No.	3. Recipient's Catalog No.
NASA CR-182023		

4. Title and Subtitle	5. Report Date
Extension of a Three-Dimensional Viscous Wing Flow Analysis	May 1990
	6. Performing Organization Code

7. Author(s)	8. Performing Organization Report No.
B.C. Weinberg, S.-Y. Chen, S.J. Thoren and S.J. Shamroth	SRA 900049-F
	10. Work Unit No. 505-63-21-01

9. Performing Organization Name and Address	11. Contract or Grant No.
Scientific Research Associates, Inc. 50 Nye Road, P.O. Box 1058 Glastonbury, CT 06033	NAS1-18140
	13. Type of Report and Period Covered: Contractor Report

12. Sponsoring Agency Name and Address	14. Sponsoring Agency Code
National Aeronautics and Space Administration Langley Research Center Hampton, VA 23665-5225	

15. Supplementary Notes

Langley Technical Monitor: James T. Howlett

16. Abstract

Three-dimensional unsteady viscous effects can significantly influence the performance of fixed and rotary wing aircraft. These effects are important in both flows about helicopter rotors in forward flight and flows about three-dimensional (swept and tapered) supercritical wings. A computational procedure for calculating such flow field is developed, and therefore would be of great value in the design process as well as in understanding the corresponding flow phenomena.

The procedure is based upon an alternating direction technique employing the Linearized Block Implicit method for solving three-dimensional viscous flow problems. In order to demonstrate the viability of this method, two- and three-dimensional problems are computed. These include the flow over a two-dimensional NACA 0012 airfoil under steady and oscillating conditions, and the steady, skewed, three-dimensional flow on a flat plate. Although actual three-dimensional flows over wings were not obtained, the ground work was laid for considering such flows. In this report the description of the computational procedure and results are given.

17. Key Words (Suggested by Author(s))	18. Distribution Statement
Viscous, two- and three-dimensional, unsteady	Unclassified - Unlimited Subject Category 02

19. Security Classif. (of this report)	20. Security Classif. (of this page)	21. No. of pages	22. Price
Unclassified	Unclassified	54	

NASA FORM 1626 OCT 86